

Mitigation urban heat island by using porous and permeable block pavement[☆]

Tiziano Dalla Mora , Giuseppe Emmi ^{*} , Paolo Ruggeri, Massimiliano De Bei, Fabio Peron 

Department of Architecture and Arts, Iuav University Venice, Italy

ARTICLE INFO

Keywords:

Climate change
Urban heat islands
Mitigation
Porous pavement

ABSTRACT

Local climate change has intensified extreme events such as the Urban Heat Island (UHI) effect, where urban areas experience higher temperatures than nearby rural zones, primarily due to the prevalence of heat-retaining materials and reduced vegetation. This creates challenges for sustainability, health, and energy use. A key mitigation method is the use of porous and permeable pavements, which enhance surface reflectivity, promote cooling through evaporation, and limit heat storage.

This study examines the performance of permeable and porous block pavements for outdoor urban applications. Field and lab measurements and ENVI-met simulations were conducted to assess various pavement types implemented in mainland Venice. Experimental tests focused on three samples—a standard block and two porous variants (dark and light-coloured) were developed to characterize the thermal properties (thermal conductivity, thermal diffusivity, solar absorptance, emissivity, and solar reflectance index) and to determine the changes in thermal fluxes during the monitoring period.

The experimental test shows how the porous light-coloured material has proved as most effective in mitigating UHI, able to reduce the average external surface temperature of by 1.5–2 °C in the afternoon in respect to the standard block; while dark porous block, even if made by the same porous material composition of light coloured, it is not always effective in improving the application due to the different albedo.

The results of the simulations are comparable to those characterised in the laboratory, with similar daily mean (almost 32 °C) and maximum (38 °C) temperatures in the receptor at the same sample location, although the daily trend is closer to that of the outdoor air.

The adoption of permeable paving blocks offers significant environmental and urban planning benefits, such as an improvement of stormwater management, thermal comfort, public health, urban liveability. Their integration into urban design could support climate resilience according to sustainability policies.

1. Introduction

The European Climate Risk Assessment recently published by the European Environment Agency has identified 36 climate risks with potentially severe consequences. European Countries have seen a constantly increasing of heatwaves, floods, wildfires and droughts, among other hazards. Europe has faced unexpected climate-related challenges, and it is warming faster than any other continent [1].

Climate change, due mainly to human activities is impacting the planet significantly. In 2023, global temperatures reached a record high, surpassing pre-industrial levels by 1.5 °C [1,2]. In the context of a global increase in temperatures, the phenomenon that occurs at a local level is

represented by Urban Heat Islands (UHI).

The UHI effect is a well-known phenomenon that can significantly impact the thermal conditions of urban areas when combined with climate change. The UHI is defined as the presence of higher temperatures in urban areas than in their rural surroundings [3,4]. This phenomenon has been identified as one of the major issues of this century [5]. In fact, the UHI is one of those consequences that have drawn attention by both researchers and stakeholders due to its harmful effects on the social and environmental stocks of global urban areas. This phenomenon is getting more intense in urban area, and it is due to several factors: growth of population, increase of construction by replacement of green areas and vegetation, increase of human-related anthropogenic activities. Consequently, the building arrangements and

[☆] This article is part of a special issue entitled: 'Countermeasures to UHI' published in Energy & Buildings.

^{*} Corresponding author.

E-mail addresses: giuseppe.emmi@iuav.it (G. Emmi), debei@iuav.it (M. De Bei), fperon@iuav.it (F. Peron).

Nomenclature	
<i>Abbreviations</i>	
UHI	Urban Heat Islands
SRI	Solar Reflectance Index, [-]
TDB	Typical Dark Block
RLB	Recycled Light Block
RDB	Recycled Dark Block
RS	Reference Scenario
AS	Analysis Scenario
<i>Symbol</i>	
L	Thickness, [m]
S	Surface area, [m ²]
ρ	Density, [kg/m ³]
λ	Thermal Conductivity, [W/(m*K)]
α	Thermal Diffusivity, [mm ² /s]
c_p	Specific Heat, [J/(kg*K)]
a	Albedo, [-]
α_s	Solar Absorptance, [-]
ε	Emissivity, [%]
v	Wind speed, [m/s]
h_c	Convection Coefficient, [W/m ² *K]
RH	Relative Humidity, [%]
T	Temperature, [°C]
T_g	Temperature gradient, [°C/m]
ΔT	Difference of Temperature, [°C]
Isol	Global Solar Radiation, [W/m ²]
Q	Energy flow, [W/m ²]
H	Sensitive Heat Flow Transmitted into the atmosphere, [W/m ²]
LE	Latent Heat Flow Transmitted into the atmosphere, [W/m ²]
G	Heat Flow Transmitted to the soil, [W/m ²]
σ	Stefan-Boltzmann Constant, [W/m ² *K ⁴]
φ	Thermal Lag, [h]
A	Attenuation, [-]
β	Phase constant, [rad/m]
f	Wave frequency, [Hz]
α	Attenuation constant, [m ⁻¹]
E	Heat Transfer, [MJ]
t	Time, [s]
<i>Subscripts</i>	
rad	Radiation
cond	Conduction
conv	Convection
sw	Shortwave
lw	Longwave
net	Net
s	Soil
0	Steady-State Surface
sur	Surface
int	Internal
ext	External
avg	Average
air	Outdoor
air10	Value at + 10 cm above surface
air100	Value at + 100 cm above surface
-10 cm	Value at -10 cm below inner surface
-25 cm	Value at -25 cm below inner surface
sky	Sky
dp	Dew Point

their characteristics are leading to temperature increases and severe heatwave effects. In addition, heatwaves have led to large energy demand due to the use of air-conditioning [1,6–9]. Furthermore, this extreme phenomenon can cause various health issues resulting in increased fatalities and illness rates [7,10].

According to United Nations Development Program, an increase of about 60 % of population is expected in large cities by 2035. Thus, the effects in climate change and UHI might enhance the vulnerability of urban environment and compromise human comfort and even worse the health of people. It is, therefore, urgent to understand in deep these issues with final aim of understand the actions to take place for the mitigation of the nowadays tendency [11,12] to preserve the near future as best as possible. Frequently the UHI is faced by using technical solutions proposed in the market, but at the same time no experimental data are available to support their validity and positive effects.

The replacement of natural surfaces by urban settlements has changed the interactions between Earth's surface and atmosphere. This change and other activities and issues may have led to alteration of urban albedo due to different thermal conductivity and thermal emissivity of urban materials than natural surfaces. A further worsening is also due to the generation of anthropogenic heat, the decrease of surface evapotranspiration in urban surface, and changes in flow character and attributes of the near-surface atmospheric processes due to low sky view factor, complex urban geometrical structures, complex street patterns, and tall building architectures [13,14]. The UHI is the result of the positive thermal balance of cities caused by the additional heat released and stored in the urban structure, and the lack of low temperature environmental sinks [15].

Pondering that, the 25 % of impervious urban surfaces is represented by paved surfaces, a sustainable and efficient replacement to traditional

pavements, usually made of cement or asphalt, could be the offer by the use of permeable pavements, also for managing the urban water runoff [16,17]. Several studies have demonstrated the effectiveness of permeable surfaces in respect to drainage surfaces to reduce the wash-off volumes. Similarly, other solutions that involve materials or modular elements paving blocks or plastic grid systems are today widely used in urban areas to create permeable areas and structures [18,19]. Although existing studies and research address this topic, further investigations and experimental activities are needed to expand and validate the effectiveness of these solutions in supporting and addressing the current climate trend and especially the UHI issue. In this context the UHI effect could be mitigated by installation of porous pavement.

Traditional paving and roofing materials absorb and store most of the solar energy that falls on the surface during the day and release it during the night, while the drainage or retention of rainwater is usually neglected or of little importance. The albedo of a pavement is the measure of the amount of sunlight reflected by a surface out of the total incident solar radiation, and it ranges from zero (corresponding to total absorption) to 100 (corresponding to a totally reflective surface). The dark surfaces that traditionally characterise the road pavements and roofs have a solar reflectance of up to 20 % [20].

The development of reflective and pervious pavement gave a significant contribute to reduce the urban temperature and to mitigate the UHI effects, through the implementation of innovative materials or the improving of solar reflection on surfaces [21–23]. Some studies analysed the possibility of mitigation of UHI by using porous mixtures materials and light-coloured surfaces [23,24].

Many studies have been published in the literature on the UHI problem and the possible measures to be taken to mitigate it. Nevertheless, as mentioned above, this area of research requires further

investigation, especially with regard to the characterisation of new materials and their use, which are not only effective but also compatible from the point of view of sustainability. Table 1 summarises some of the research that has been carried out in this area and suggests possible solutions. The table briefly describes the content and results of the studies. For each research, the methodology and the topic on which the work is focused are reported. As can be seen from the table, the studies focus on the surface properties of pavements or on the use of devices embedded in the pavement itself that affect the surface temperature of the pavement. The table above includes a reference to the methodology used in the research as well as the main topic of the work. The list given is not intended to be exhaustive, but it is meant to be a reference of possible actions to mitigate the UHI.

Differently to the findings of previous studies documented in Table 1, an alternative approach for mitigating UHI involves the enhancement of cooling evaporation through the implementation of permeable pavement solutions. For this aim the structure must need porous layers on the pavement with a consequently change in thermal resistance properties of the pavement layers if compared to the traditional pavements in concrete or asphalt. The complexity of the different phenomenon which acting together requires a deep knowledge and experience to clearly understand positive and negative aspects. In fact, the research on this topic for the UHI mitigation show mixed results frequently discordant. A list of studies related the use of porous and permeable pavements are summarized in Table 2. The structure of the table is equal to the previous Table 1.

As shown in Table 2, the use of porous and permeable materials gives different results depending on the conditions of use. In particular, resuming the contents analysed in the table, while some studies found porous concrete blocks effective in reducing potential air temperature by -1.26 °C [33], others reported increased daytime air temperatures with porous asphalt and concrete [35]. Porous pavements generally exhibit lower nighttime temperatures compared to traditional materials due to their insulating properties [36]. However, their effectiveness may vary depending on urban layout and environmental conditions [35]. Porous pavements typically reflect less heat than traditional concrete, potentially reducing thermal discomfort for nearby humans and buildings [39]. The impact of porous pavements on UHI is complex, involving interactions between factors such as pavement thickness, structure, material type, and albedo [36]. Further research is needed to evaluate porous pavement applications in experimental and real case studies to evaluate the effectiveness in mitigating UHI under various urban conditions.

As evident from the preceding analyses, modifying the properties of the pavement surface consistently yields predictable results. However, altering pavement behaviour by adjusting its porosity and permeability does not always produce the expected outcome.

This present paper summarized the results of experimental and simulation activities of the study on a permeable pavement block produced with recycled natural stone. This innovative and eco-friendly material has the target to reduce urban water runoff and UHI, because of the porous structure and the light-coloured surface. Furthermore, the novelty of the material lies in its ability to reduce the rise in surface temperature: the cavities make it possible to increase the surface of shaded areas and to store rainwater, favouring a convective heat exchange and a slow evaporation.

While not the focus of this study, this latter aspect could be of significant importance, as evidenced by recent substantial scientific studies on Life Cycle Assessment dedicated to permeable pavements (concrete or porous asphalt) incorporating recycled aggregates, with a focus on environmental benefits [40–43].

The integration of permeable paving blocks into urban design represents a multifaceted strategy with significant environmental, social, and policy-related implications.

In fact, these systems are characterized by high capacity to allow water infiltration and reduce surface runoff and they offer not only

Table 1

Set of research studies on reflective properties of the pavements, retain water capability and use of embedded devices.

Authors and Reference	Year	Methodology	Description	Topic
Battista et al. [25]	2023	Monitoring Activities and Simulation	<ul style="list-style-type: none"> • A square in Rome as case study. • Study focused on calibrating the model, not testing proposed solutions. • Grass pavers identified as the most beneficial solution. • Lower air temperature was obtained: up to 2.5 °C in the center of the square, up to 1 °C in surrounding areas. 	Surface properties
Susca et al. [26]	2023	Simulation	<ul style="list-style-type: none"> • Green roofs, green façades and living walls were investigated. • Study areas in urban zones (Turin and Rome). • Effectiveness by average temperature reduction of up to 1 °C in the built areas. • Simulations by ENVI-met tool method. 	Surface Properties
Governatori et al. [27]	2022	Experimental	<ul style="list-style-type: none"> • Reflective materials help mitigate the UHI effect. • Modifying engobe formulation alone is insufficient for achieving high solar reflectance in ceramic tiles. • Solar reflectance improved from 0.69 (standard product) to 0.75 (experimental product). 	Surface Properties
Shimazaki et al. [28]	2022	Experimental Activities	<ul style="list-style-type: none"> • Reflective and water-retaining pavements have been optimized for cooling. • Comparison made between optimized and conventional pavements. • No measurable effect of water-retaining pavements on air temperature and humidity at pedestrian height found in the experiment. • Cooling effects of reflective (cool) pavements consistent with 	Surface properties combined with water retain

(continued on next page)

Table 1 (continued)

Authors and Reference	Year	Methodology	Description	Topic
Chen et al. [29]	2019	Experimental Activities	<ul style="list-style-type: none"> findings in existing literature. Field albedo measurements influenced by solar radiation intensity, incident angle, and surrounding conditions. Albedo and temperature of asphalt mixtures with and without reflective coatings measured and compared. Reflective coatings significantly increased albedo (from 5–6 % to 22–26 %). Coatings also reduced the temperature of the asphalt mixtures. 	Surface Properties
Chiarelli et al. [30]	2017	Experimental Activities and Simulations	<ul style="list-style-type: none"> Embedded pipes for air heat exchange are used. Effects: winter – temperature increases by 0.4 °C to 2.1 °C., summer – temperature decreases by 2 °C to 6 °C. 	Embedded devices in the pavement
Anting et al. [31]	2017	Experimental Activities	<ul style="list-style-type: none"> Cool pavements with waste tile aggregates (pure or mixed). Pure “Full Body Porcelain” showed the best performance, reducing surface temperature by up to 6 °C during peak times. 	Surface properties
Carnielo and Zinzi [32]	2013	Monitoring Activities and Simulations	<ul style="list-style-type: none"> Cool materials tested on asphalt and pavements. Optical and thermal properties analysed in labs and outdoor settings. The impact of road albedo on air temperature was evaluated. 	Surface properties

hydrological benefits but also contribute to the mitigation of the UHI effect. By enhancing evaporative cooling and increasing surface albedo, permeable pavements help lower ambient temperatures in urban areas—a function that becomes increasingly critical in the context of global warming and the densification of cities [44].

In urban planning activities the permeable pavements are recognized as integral components of Nature-Based Solutions, which aim to address societal challenges through the application of natural processes (European Commission, 2021) [45]. Their adoption is also consistent with the EU Water Framework Directive (2000/60/EC) [46], which requires member states to achieve “good” water status by managing urban runoff and reducing pollutants entering water bodies. Furthermore, the Floods

Table 2

Set of research studies on porous and permeable pavements.

Authors and Reference	Year	Methodology	Description	Topic
Ranieri et al. [33]	2022	Simulation	<ul style="list-style-type: none"> Simulations conducted in a parking area in Bari, Italy. Six different pavement materials tested. Air temperature reduction: green pavement – 1.22 °C, grey porous concrete blocks – 1.26 °C, light concrete permeable pavement – 1.22 °C. 	Porous pavement
Chen et al. [34]	2019	Experimental Activities	<ul style="list-style-type: none"> High-conductivity permeable concrete pavement has been tested Surface temperature reduction: by 1 °C to 3 °C compared to conventional permeable concrete. Dry conditions: higher surface temperature than conventional type. Wet conditions: similar or lower surface temperature than conventional type. 	Porous pavement and thermal conductivity
Coseo et al. [35]	2015	Experimental Activities	<ul style="list-style-type: none"> The study evaluates two cool paving strategies. Porous pavement not significantly cooler during dry or wet periods. Porous asphalt and concrete increased daytime temperatures by 0.8 °C and 0.5 °C, respectively. Porous or highly reflective pavement did not reduce nighttime air temperatures. 	Porous pavement
Stempihar et al. [36]	2012	Experimental Activities	<ul style="list-style-type: none"> A pavement temperature model used to study surface temperatures of various materials. Porous asphalt had higher daytime surface temperatures than other pavements. At night, porous asphalt showed the lowest temperatures compared to other 	Porous pavement

(continued on next page)

Table 2 (continued)

Authors and Reference	Year	Methodology	Description	Topic
Haselbach et al. [37]	2011	Experimental Activities	<p>materials with similar albedo.</p> <ul style="list-style-type: none"> • Pervious concrete had a lower Solar Reflectance Index (SRI) than traditional concrete but can still function as a cool pavement. • Daytime rainfall combined with high internal surface area helped remove stored heat quickly, reducing UHI effects and thermal shock from runoff. • Daytime rain caused significant heat reduction, unlike nighttime rain. • Stored rainwater in pervious concrete cooled the pavement through evaporation, enhancing heat mitigation. 	Porous pavement
Asaeda and Ca [38]	2000	Experimental Activities	<ul style="list-style-type: none"> • Mechanisms to control thermal behaviour of urban pavement and wall materials were investigated. • Studied use of porous materials to enhance water exchange between surface and deep soil. • Porous pavement surfaces showed lower temperatures than non-porous and standard porous block pavements. 	Porous pavement and water evaporation

Directive (2007/60/EC) [47] encourages the use of Sustainable Urban Drainage Systems (SUDS), of which permeable surfaces are a core element, to improve climate resilience.

Empirical examples underline the practical relevance of this approach. Copenhagen, under its Cloudburst Management Plan [48], has widely integrated permeable pavements into public spaces to reduce flood risks while improving the urban microclimate. Likewise, Portland, Oregon's Green Streets Program [49] uses permeable infrastructure to alleviate pressure on its combined sewer system, demonstrating the dual role of these surfaces in water management and urban greening.

Similar strategies have been implemented in cities such as Berlin and Tokyo. In Berlin, the city's Rainwater Agency (Berliner Regenwasseragentur) has promoted the large-scale deployment of permeable pavements through financial incentives and regulatory frameworks, significantly reducing stormwater runoff and supporting groundwater recharge, particularly in retrofitted courtyards and schoolyards [50]. Tokyo's Sumida City has adopted permeable block pavements across its public spaces since the early 2000s, aiming to mitigate localized flooding and enhance thermal comfort. Studies have demonstrated that these

interventions led to measurable reductions in surface temperatures and improved infiltration capacity during peak rainfall events [51]. These cases highlight how permeable paving can be adapted across diverse climatic and regulatory contexts, reinforcing its relevance as a resilient infrastructure solution.

Permeable pavements also hold public health significance. By lowering surface temperatures in pedestrian-heavy environments, they reduce the exposure of vulnerable populations to heat stress, a factor increasingly emphasized in urban health policies (WHO, 2021) [52]. Moreover, their deployment can enhance urban aesthetics, encourage walkability, and improve the quality of public spaces—thus aligning with the objectives of the United Nations' Sustainable Development Goal 11: "Make cities and human settlements inclusive, safe, resilient and sustainable" [53].

This study examines the performance of permeable and porous block for outdoor pavements with the aim to evaluate the effectiveness as application to mitigate UHI. Field and lab measurements and ENVI-met simulations were conducted to assess various pavement types implemented in a common case study (the mainland Venice). This study represents a novel contribution to the research field, as previous research and literature analysis has largely focused on either laboratory analysis or simulations. The paper is structured as following. The methodology section describes the developed research, introducing the study area and the analysed components, describing the activities carried out in the laboratory on different pavement blocks, and lastly describing the development and setup of the simulation model to analyse the behaviour of the new permeable block in comparison with common ones in real case. The next section reports and compares the results of experimental tests and model simulations. Lastly the conclusions about the main findings of the research are described.

2. Methodology

The present section reports in detail the experimental and simulations activities regarding the application of so-called "cool pavement" in urban area. In particular, the first part presents the Recycle porous block and its main characteristics; then the second part is dedicated to a general overview of the study area and the location of the experimental test. The third part describes the activities conducted for the characterization of a new porous block used for urban pavement, giving an overview of the results of the laboratory measurement, and describes the arrangement of the mock-ups for experimental test. Some international standards were taken as reference for the characterization of the porous blocks and the most relevant results and performance indicators were calculated. The fourth part shows the application of porous block in a real case study by means of numerical simulations. The simulation model is developed using the same monitoring data gathered from the experimental activities and represents the same urban area in which the experimental tests have been carried out.

2.1. The recycle porous block

The specific construction element used for this study is a porous and permeable pavement block, hereafter named Recycled Block, a picture of the block is reported in Fig. 1. The geometric dimensions of the block are 100*20*8 cm, volume 0.017 m³ and density 1824 kg/m³. For experimental test two different versions of block are adopted, a dark coloured surface (reported in Fig. 1) and a light coloured one.

The block material includes recycled aggregates in reclaimed porphyry or agglomerates of rock origin, bound with small amounts of concrete. The material consists of an isotropic distribution of the voids in the porous structure, about 15–20 % empty spaces of the total volume, which allows permeability coefficient equals at 3.27*10⁻³ m/s at 10 °C.

The choice of this type of product for the research concerns the innovative aspects of the product itself and the circular aspect linked to the use of purely recycled material. In particular, it helps to solve the



Fig. 1. Example of Recycle® porous block (dark version).

issues related to soil sealing, allowing the exchange of water vapour and heat through its surface. Its permeability enhances water infiltration in the subsoil and the next collect to the edge of the collecting area, at the same time it allows and promotes an easier residual water evaporation in the various substrates between its layers, contributing to counteract both flash flooding and droughts. Its structure also reduces the amount of heat stored during the day and increases the evaporative cooling, counteracting UHI effects.

2.2. The case study area

The case study refers to an urban zone of Venice mainland in Italy, already investigated in a previous research [54]. It regards the university district of Via Torino in Mestre (45.26 N 12.19 E), Italy, placed at 3

m height above sea level; it concerns on a new urban mixed area comprising residential, office, commercial, wholesale market, and hotel and university buildings. The area, approximately 486.000 m², lies in the southeast section of Mestre among the city centre, the railway lines connecting Venice with the mainland and San Giuliano public park close to the lagoon. The site is crossed from north by the “Canal Salso” canal, which is the water route running into the Venice Lagoon. Fig. 2 shows an aerial photograph of the site (highlighted in red) and the surrounding area; the black dot indicates the placement of the area where the samples were placed for the experimental part and the investigation area for the numerical simulation, as better defined in the next paragraphs and in Fig. 3 and Fig. 4.

Venice climate is classified as Cfa according to the geographical location and related climatic classification by Köppen e Geiger [55], characterized by has a humid subtropical climate that is mild with no dry season, constantly moist (year-round rainfall). Summers are hot and muggy with thunderstorms. Winters are mild with precipitation from mid-latitude cyclones. The urban area of Mestre presents climatic conditions given by weather station Venice airport, geographical coordinates 45°29'43.29"N 12°20'30.4"E; as reported in the Atlante Climatico d'Italia edited by Servizio Meteorologico dell'Aeronautica Militare [56], this urban area experiences historical trend with mean annual temperatures between 17.2 °C and 8.8 °C, mean annual relative humidity from 72 % to 80 %, with rainfall varying from 48 mm to 78 mm.

This study considers a more detailed climatic reference, using the data of the environmental meteorological monitoring station located at the site of the Building Physics Laboratory [57] of the IUAV University of Venice (Geographical Location: N 45°28'47.68", E 12°15'18.19"), placed properly in the study area. Wind speed and direction, solar radiation, rain, air temperature and relative humidity are measured at a height of 10 m. The extracted data for 2018 have been considered and used for the thermal characterization of the specimens (in particular for solar reflectance measure) and for the experimental test in the mock-ups to



Fig. 2. Satellite view of Mestre: the red line underlines the study case along the via Torino university district (45.49° N, 12.24° E). The black dot indicates the placement of the area where the samples were placed for the experimental part and the investigation area for the numerical simulation, better described in Fig. 3 and Fig. 4. (For interpretation of the references to colour in this figure legend, the reader is referred to the web version of this article.)



Fig. 3. Aerial view of the urban zone close to the experimental area in red; the blue icon indicates the position of the photographic point of view of Fig. 4 and the placement of the local meteorological monitoring station used for this study. (For interpretation of the references to colour in this figure legend, the reader is referred to the web version of this article.)

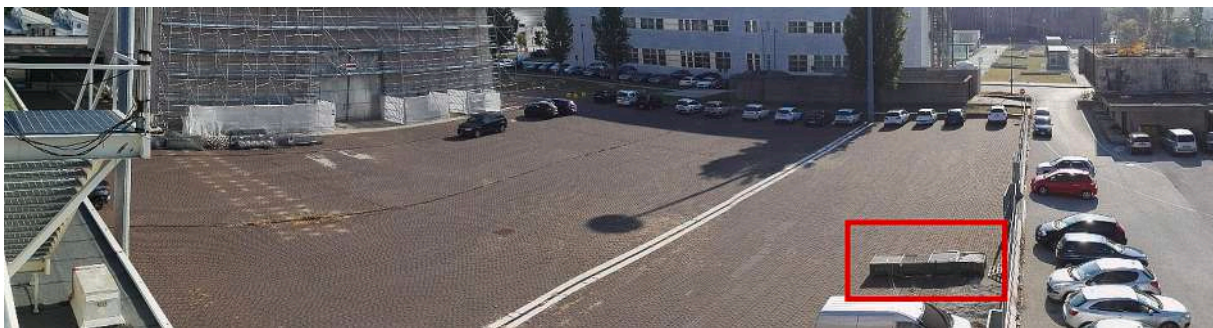


Fig. 4. View of the study area with the installation of porous block in substitution of standard block. The red frame identifies the location of the samples built for the thermal characterization tests. (For interpretation of the references to colour in this figure legend, the reader is referred to the web version of this article.)

evaluate temperature trend and heat flux. The data recorded for 2018 gives some differences in respect to the historical data: the temperatures vary between a minimum $-5\text{ }^{\circ}\text{C}$ recorded on February to $36\text{ }^{\circ}\text{C}$ on August, mean daily relative humidity from 57 % to 91 %, with rainfall varying from 0.2 mm to 23 mm, wind speeds averaged is 1.45 m/s, the radiation has a daily average of 170 W/m^2 and annual global radiation is 1460 kWh/m^2 .

Currently the university district is characterized by limited density, medium height buildings and it can be classified as “open midrise” with paved land (Local Climate Zone 5E) [58]. However, a new urban redevelopment plan has been activated to renovate the open spaces and renovate the existing buildings: the plan established the redevelopment of the old market and the Cà Foscarelli University campus expansion with the construction of new buildings for host research laboratories and teaching activities.

As mentioned before in the text, the experimental test has been developed in the parking area in front of the LabSCo Laboratory of Strength of Materials of IUAV University of Venice near the Building Physics Laboratory. This same parking area has been used in the numerical simulations as the surface subject to replacement of the existing flooring with the one being investigated in this work, as better detailed in the next section. Two pictures of this area are reported in Fig. 3 and

Fig. 4.

2.3. Laboratory and experimental tests

This section describes the works carried out in the Building Physics Laboratory (FisTec Lab) of the University IUAV of Venice divided into laboratory and experimental activities respectively. The laboratory tests were performed before the field measurements to characterize the specimens’ thermal properties, such as thermal conductivity, thermal diffusivity, solar absorptance, emissivity, solar reflectance index (SRI), and temperatures of the block under operating conditions. The results of this part of the work are summarized in the present section. The Table 3 depicts the instruments and devices used for laboratory tests.

As mentioned before, the study of the behaviour of Recycled Blocks is the focus of this study. In particular, two different Recycled block types with thickness 8 cm have been used in the tests and they were compared with a common block type present in the market. In the following the Typical Dark Block is named TDB, the Recycled Light Block and the Recycled Dark Block are named RLB and RDB respectively. The pictures of the blocks are reported in Fig. 5.

To deeply investigate the thermal characteristics and the behaviour to solar stresses, the experimental activity has been proceeded with the

Table 3

List of instruments of the Building Physics Laboratory (FisTec Lab) of the University IUAV of Venice used for the experimental tests.

Physical quantity measured	Instrument	Sensor image	Specifications and accuracy
Air Temperature [°C] (+10 m height)	Thermohygrometer LSI DMA533		Range $-30 + 70$ °C; 0–100 % Rel. Accuracy: $T \pm 0,15$ K @ 0 °C, RH 1 % (10... 30 °C)
Global Radiation [W/m ²]	Radiometer L Delta Ohm P PYRA 10		Spectral range: 305–2800 nm (50 % points) Sensitivity: $10 \mu\text{V}/\text{Wm}^{-2}$ Impedance: 500–1000 Ohm Non linearity: $< \pm 0,5$ %
Global Radiation [W/m ²]	Pyranometer CM 6B		Spectral range: 305–2800 nm (50 % points) Sensitivity: $9\text{--}15 \mu\text{V}/\text{Wm}^{-2}$ Impedance: 70–100 Ohm Non linearity: $< \pm 1,2$ % ($< 1000 \text{ W}/\text{m}^2$)
Thermal Conductivity [W/mK], Thermal Diffusivity [mm ² /s], Specific Heat Capacity [MJ/m ³ K]	Transient Plane Source device, HotDisk AB 2500		Thermal Conductivity: 0.005 to 500 W/mK Thermal Diffusivity: 0.1 to 100 mm ² /s Specific Heat Capacity: Up to 5 MJ/m ³ K Accuracy: Better than 5 %
Temperature [°C]	PT100 class A4-wire temperature		Accuracy: $\pm(0,15 \text{ °C} + 0,2 \text{ % of temperature})$

construction of test facilities that reproduce the flooring in real conditions. Three mock-ups have been built and placed on the parking pavement close to the laboratory (see Fig. 4). Some pictures of the installation are reported in Fig. 6.

Fig. 7 shows pictures and schemes of the measuring system. The blocks were placed on a 30 cm layer of gravel in thermally insulated plastic containers. The container is 100*100*58 cm and it consists of a green high-density polyethylene HDPE parallelepiped ($\lambda = 0.5 \text{ W}/(\text{m}^*\text{K})$, $\rho = 970 \text{ kg}/\text{m}^3$) lined with 5 cm of white Sintered Expanded Polystyrene EPS ($\lambda = 0.034 \text{ W}/(\text{m}^*\text{K})$, $\rho = 27.8 \text{ kg}/\text{m}^3$) for thermal insulation, filled with sand commonly used as a street substrate (diameter 4–6 mm, $\lambda = 0.152 \text{ W}/(\text{m}^*\text{K})$, $\rho = 1331.3 \text{ kg}/\text{m}^3$). In each installation, 5 PT100 class A 4-wire temperature sensors were placed to monitor the response to stress. The sensors were linked to a datalogger (a Thermo Fisher Scientific DataTaker DT80 Series Data Logger) placed in the laboratory room. The 5 sensors were installed along the vertical axis (as shown in Fig. 7 b and d) with #1, #2, #3 and #4, respectively above the surface of the tiles, below their inner surface, at a depth of 10 cm and a depth of 25 cm. In addition, a PT100 sensor was placed at 10 cm above the external surface (#air in Fig. 7 d) of the samples to measure the overlying air temperature.

The sample preparation followed this process shown in Appendix 1:

supply and installation of the 3 containers, arrangement of the polystyrene panels in each container, arrangement of the gravel sand up to the 0 level alternating the position of sensors #4, #3, #2 (as shown in Fig. 7 b and d) at different levels; arrangement of the 3 sample types and of the external sensor #1 in adherence to the external surface of the specimens; placement of the external sensor #air.

The monitoring period for the experimental test has been lasted from 11/09/2018 (at h 16:00) to 01/10/2018 (at h 7:00), the temperatures have been recorded by PT100 sensors with a time step of 10 min. The boundary conditions of the site where the tests were carried out were processed from the data recorded by the aforementioned meteorological station of the Building Physics Laboratory of the IUAV University of Venice located in the study area; along the same monitoring period the measured variables considered were temperature, relative humidity and global solar radiation, with a time step of 10 min.

The thermal properties have been measured through the laboratory tests for two samples (the TDB and the RLB) by means of HotDisk AB 2500 TPS device [59,60], equipped with sensor HD-SENS-K-D8563 of radius 9.9 mm. The declared accuracy of the device is better than 5 % and the main specifications of the device are reported in Appendix 2.

The experiments on the samples were performed at constant room temperature (23 °C), the input power was set at 0.14025 W and the

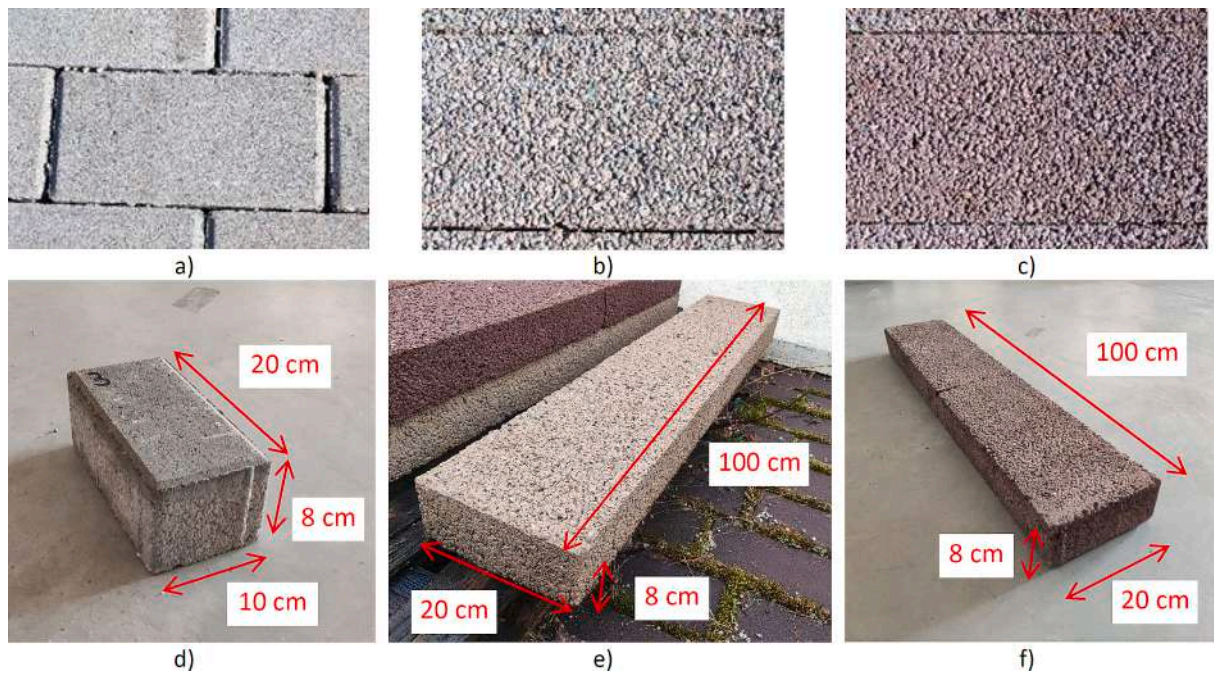


Fig. 5. Experimental specimens for laboratory characterization: a) and d) Typical Dark Block, TDB; b) and e) Recycled Light Block, RLB; c) and f) Recycled Dark Block, RDB.

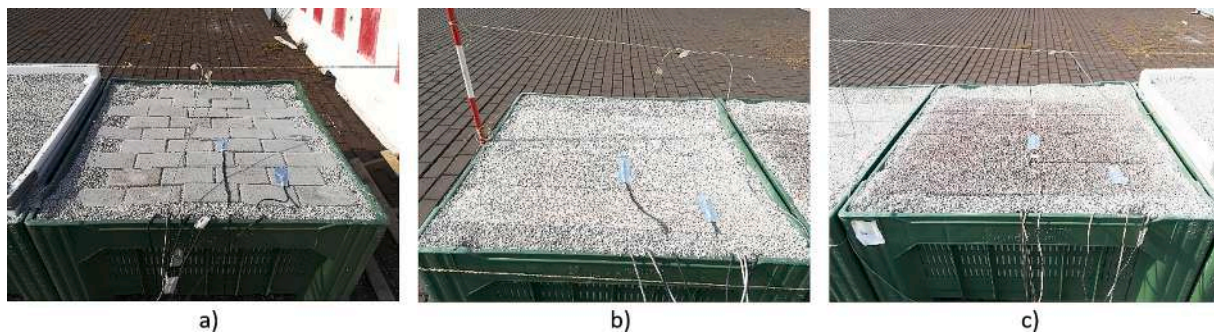


Fig. 6. Experimental setup: a) TDB; b) RLB; c) RDB.

measuring time lasted 160 s. Other parameters used for experiments are listed in Appendix 3.

The applied methodology refers to the Transient Plane Source Method, according to the standard ISO 22007-2:2022 [60]. In detail, a sensor is placed between two halves of the sample to be measured; during the measurement a constant electrical effect passes through the conducting spiral, increasing the sensor temperature. The heat generated dissipates into the sample on both sides of the sensor, at a rate depending on the thermal transport properties of the material. By recording temperature vs. time response in the sensor, the thermal conductivity, thermal diffusivity and specific heat capacity of the material can be calculated. The setup for this kind of experimental test contemplates that the sensor should be locked between samples to ensure a thermal contact and moreover that the sample surfaces in contact with the sensor should be flat and smooth; for this reason, due to the highly porous external surface, the Recycled sample was cut and smoothed to obtain a flat surface. In fact, for this test the dimensions of the three samples have been reduced to 10x10x8 cm.

A series of measurements were performed in the samples by moving the analysis point, resulting in the values reported in Table 4 with accuracy lower than 5%.

The two samples present similar values of thermal conductivity λ (difference rate -4%), 1.80 W/(m²K) and 1.73 W/(m²K) for TDB and

for RLB respectively. The main difference consists in the values of thermal diffusivity α (difference rate -31%) and specific heat c_p (difference rate 65%), due to the different densities (16% lower in RLB) and the volumetric heat capacity (greater in RLB).

The thermal diffusivity, which is lower for the RLB than for the TDB, is useful in describing the transport of heat in a semi-steady state. Under such conditions with similar density and thermal conductivity values, the material effectively transmits heat flow due to its low specific heat. Therefore, the RLB material has a lower capacity to absorb heat and store it within the layer.

Moreover, the SRI values of the three samples that affect UHI phenomenon have been evaluated by means of measurements. The SRI is a parameter that measures the ability of a material to reflect incident solar radiation. It is a normalised measurement unit, obtained according to a standard defined by ASTM E1980-11 [61], ASTM E1918-06 [62], that combines solar reflectance (SR) (the capacity of the material to reflect solar radiation), the thermal emissivity (ϵ) and the heat released by the material. In summary, SRI indicates the capacity of a material to thermally insulate a substrate or surface from exposure to sunlight. Thus, a material with a higher SRI has a lower increase in its temperature when exposed to solar radiation, and the surface exposed to solar radiation will remain "cool".

Solar reflectance is a measure of the fraction of incident solar

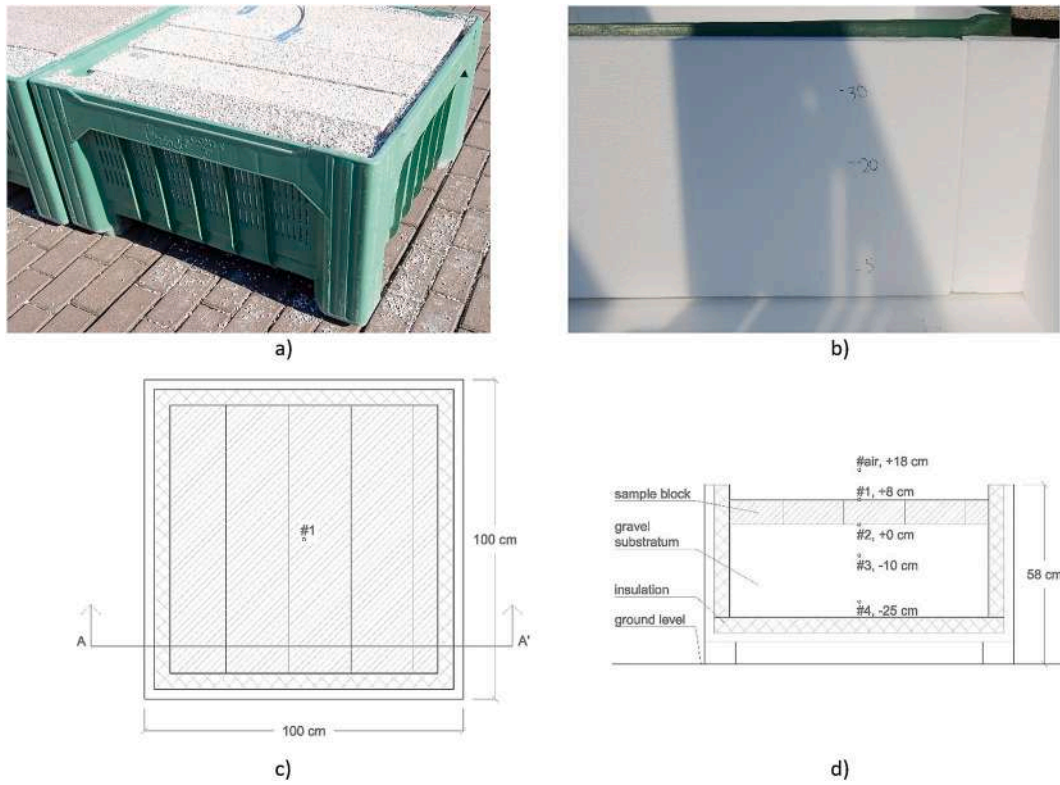


Fig. 7. Main views of the test facilities and drawings: a) External view; b) Internal View; c) Drawing of the plan view; d) Drawing of the section AA' of the system with the position of the PT100 temperature sensors.

Table 4
Thermal characterization by test according to Transient Plane Source Method and standard ISO 22007–2:2022, by means of HotDisk AB 2500 TPS device.

Sample	TDB	RLB/RDB	Difference
ρ [kg/m ³]	2168	1824	-16 %
λ [W/(m ² K)]	1.8	1.73	-4%
c_p [J/(kg ² K)]	634	1045	65 %
α [mm ² /s]	1.31	0.91	-31 %

radiation that is reflected by an irradiated surface. The value varies between 0 and 1, a totally absorbing and a totally scattering surface respectively. The closer the reflectance value is to 0, the less the material has the capacity to reflect solar radiation.

According to standard ASTM E1918-06, the solar reflection coefficient of three samples (already described in Fig. 6) has been measured by a Kipp & Zonen model CM 6B pyranometer [63], mounted on a 30 cm high tripod from sample's inner surface and connected to a Datataker 605 multi-channel data acquisition system. The main technical data

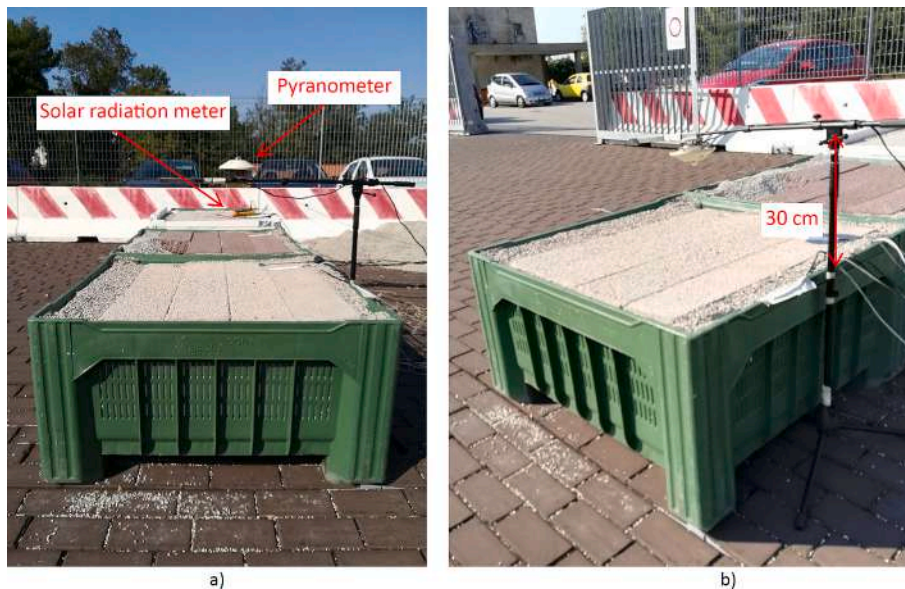


Fig. 8. Instrument for SRI characterization: a) pyranometer, b) layout of the measurement system according to standard ASTM E1918-06, c) and d) placement of pyranometer for testing the three samples.

specifications of the pyranometer are summarized in Appendix 4. A picture and a scheme of the measuring system are reported in Fig. 8.

The average of the solar radiation was measured with the pyranometer facing the celestial vault for a period of 3 min and a data acquisition time of time of 5 s, continuing with the measurement of the surface reflection with the pyranometer facing the surface of the sample. The measurements with the pyranometer were carried out on 19/10/2018 at h 12:00.

The solar reflection coefficient is calculated as the ratio between the two aforementioned values or between the value of solar radiation and the value of the radiation reflected by the surface.

Thermal emissivity, on the other hand, is the fraction of energy radiated by the material relative to the energy radiated by a black body at the same temperature and takes on values between 0 and 1. It depends on factors such as temperature, emission angle, wavelength and surface finish of the observed body.

The emissivity measurement was performed according to the ASTM C1371-15 Standard [64] with an emissometer Device and Service model AE1.

The standard for SRI calculation requires the evaluation of the performance of the elements of the shell with respect to the absorption and re-emission of energy, with reference to two standard surfaces: standard white (SRI = 100), with solar reflection coefficient 0.8 and thermal emissivity 0.9, and standard black (SRI = 0), with solar reflection coefficient 0.05 and thermal emissivity 0.9.

According to standard ASTM E1980-11, for this test insolation and environmental conditions are set as following: global solar radiation 1000 W/m^2 , ambient temperature 310 K, sky temperature 300 K, convection coefficient (h_c) as $5 \text{ W/m}^2\text{K}$ in case of low wind speed ($0 \div 2 \text{ m/s}$), $12 \text{ W/m}^2\text{K}$ for average wind speed ($2 \div 6 \text{ m/s}$), $30 \text{ W/m}^2\text{K}$ for high wind speed ($6 \div 10 \text{ m/s}$).

Under these standard conditions the SRI coefficient is given according to the Equation (1):

$$\text{SRI} = 123.97 - 141.35\chi + 9.655\chi^2 \quad (1)$$

where:

$$\chi = \frac{(\alpha_s - 0.029\varepsilon)(8.797 + h_c)}{9.205\varepsilon + h_c}$$

α_s = solar absorptance, 1 – solar reflection, [-]

ε = emissivity, [%].

h_c = convection coefficient, [$\text{W}/(\text{m}^2\text{*K})$].

The 3 samples have been tested. The results are reported in Table 5.

Given the measured values of solar absorptance α_s [-] and emissivity ε [%], the SRI is calculated for the considered 3 wind speeds giving 3 results with the same round value, so for this study the SRI index calculation considers the average value rounded. As it can be seen in the table the RLB obtained a slightly better SRI value (35 %) than that of the TDB (32 %), due to the higher value of solar reflection coefficient (31 %) and emissivity (93 %). Despite the similar emissivity (93 %), the RDB instead presents a low SRI value (18 %) due to the dark colour and the relative temperature of the surface. The calculation report values of steady-state surface temperature (T_0) higher for RDB ($75 \text{ }^\circ\text{C}$) than RLD and TDB (close $70 \text{ }^\circ\text{C}$).

After making the reflectance measurements, the field experiment has

Table 5

Values given by the test for solar reflection coefficient calculation, by means of Kipp & Zonen model CM 6B pyranometer.

Sample	TDB	RLB	RDB
α_s [-]	0.71	0.69	0.82
ε [%]	92	93	93
T_0 [$^\circ\text{C}$]	70	69	75
SRI_{avg} [%]	32	35	18

been carried out on the three mock-ups, with the aim of determining the thermal behaviour of the samples on a real case.

2.4. Simulations

This section reports the details of the microclimatic numerical model developed, describing the main characteristics of the ENVI-met tool [65], the boundary conditions adopted in the numerical model, the modeling of the porous block RLB and the definition of the two simulated scenarios, a so-called Reference Scenario (named RS) and an Analysis Scenario (named AS).

This part of the research is intended to provide a complementary evaluation of the experimental approach previously outlined. The objective is to assess the potential implementation of a porous recycled pavement material in a real context. A numerical model in ENVI-met, implemented with properties and values obtained from laboratory measurements on the samples, was adopted to facilitate a comparison between the real state and a hypothetical scenario on the warmest day of the year (02/08), chosen in order to investigate the mitigation effects of UHI in the worst temperature climate situation of the year.

The integration of these two aspects is further facilitated by the fact that the study area in the numerical model corresponds to the location where the mock-ups of the experimental analysis were installed.

2.4.1. Properties of the simulation model

The simulations have been carried out by using ENVI-met v.4.3, Winter1718, a comprehensive microclimate simulation software used for urban climate modeling, thermal comfort analysis, and environmental planning. [66]. It consists of several key modules, each serving a specific function: “Monde” is a visualization and analysis tool for reviewing simulation results in 2D and 3D; “Spaces” is the graphical user interface for setting up simulation areas and configurations; “ENVI-Guide” serves as the main control centre for managing ENVI-Met projects and it provides an organized workflow for setting up, running, and analysing simulations; “ENVI-Core” is the central simulation engine and it handles physics-based calculations related to microclimate, such as airflows, radiation, soil temperature, vegetation processes, and pollutant dispersion; “Leonardo” allows the post-processing and visualization of simulation results; “BioMet” is a tool for calculating human thermal comfort indices like Predicted Mean Vote PMV. Moreover, two main databases are present: “Albero” is the database for managing plant and vegetation parameters and properties; “Database Manager” allows users to manage and edit different environmental and material datasets used in simulations. It is accessible through ENVI-Guide and helps in customizing the input parameters for vegetation, soil, buildings, and atmospheric conditions. Last the “Forcing Manager” is another important component, used for defining and modifying external meteorological conditions in order to create realistic and dynamic microclimate simulations.

Specifically, it can simulate a three-dimensional non-hydrostatic microclimate model SVAT (Soil, Vegetation, Atmosphere, Transfer). It is designed for microscale analysis with a typical horizontal resolution from 0.5 m to 5 m and a typical simulation period between 24–48 h with a time step between 1–5 s: this resolution allows to analyse small-scale interactions between buildings, surfaces and vegetations in the investigated area.

This study upgrades a simulation model used in the aforementioned previous model [54], the details and settings of the model for ENVI-met simulations are summarized in the following and reported in Table 6.

The modelling started with converting two-dimensional maps from GoogleMaps into a three-dimensional model. The calculation grid is sized $900(x)$, $540(y)$, $49.5(z)$ m (being z the vertical axis), the number of cells is $180(x)$, $105(y)$, $25(z)$.

Afterwards, in “Spaces” module details of the buildings and surfaces were added according to the materials properties defined by default or by user in the Database Manager. Details such as the location and size of

Table 6
Model details and settings and boundary conditions for ENVI-met simulations.

Parameter	Value
Software and version	Version 3
Computation domain	900(x) * 540(y) * 49.5(z) m
Basic cell size	5(dx) * 5(dy) * 2(dz) m
Number of grid cells	180 * 108 * 25 (W * L * H)
Near-ground grid cells	Divided into five sub-cells
Model rotation out of grid north	40.0 deg
Simulation site	Venice, Italy, 45.26 N 12.19 E
Name of reference time zone	CET/GMT + 1
Definition longitude of time zone	15.00
Weather data (longwave radiation, direct shortwave radiation, and diffuse shortwave radiation)	Default location-specific values provided by ENVI-met
Weather data (air temperature, relative humidity, wind speed, and wind direction)	Weather station of Building Physics Laboratory of IUAV University of Venice
SIMULATION DATA	
Start Simulation at Date	01/08/2018
Start Simulation at Time	6:00 a.m.
Total simulation time [h]	42
Save Model State each? min	60 min
Wind Speed at 10 m ab. ground	0.66 m/s
Wind Direction (0:N, 90:E, 180:S, 270:W)	20, NE
Temperature	295 K
Relative Humidity in 2 m	64 %
Specific humidity at 2500 m	7 $g_{\text{water vapor}}/kg_{\text{air}}$
Roughness length at measurement site	0.1 m
SOIL	
Albedo of soil and pavements (-):	
- waterproof asphalt (reference scenario RS)	0.06
- waterproof cement (reference scenario RS)	0.13
- porous block (analysis scenario AS)	0.31
BUILDING	
Inside Temperature	Costant, 293 K
Heat Transmission Walls	0.8 W/(m ² K)
Heat Transmission Roofs	1.2 W/(m ² K)
Albedo Walls	0.35
Albedo Roofs	0.05

trees were based on the “Albero” database. Regarding the albedo values employed in this simulation model for soil and pavement, it should be specified that for waterproof asphalt and concrete utilized for the reference scenario (designated RS), the default data incorporated in the ENVI-met material database is adopted. For the Recycle porous material pavement, utilized for the analysis scenario (designated AS), the albedo value is determined through laboratory and experimental tests data, as outlined in the previous sections, so it refers to the properties of Recycled blocks RLB specimen.

The boundary conditions of air temperature, wind speed, relative humidity have been set and implemented in the “Forcing Manager” module, according to weather data obtained from the field measurement and data collected by the meteorological station of Building Physics Laboratory of IUAV University of Venice, while default location-specific values provided by ENVI-met are used for other weather data (longwave radiation, direct shortwave radiation, and diffuse shortwave radiation).

After model, numerical simulations were conducted by using “ENVI-guide running” and “ENVI-core” by fixing the analysis of the two different scenarios at the 02/08 as the warmer summertime day.

2.4.2. The simulation model of the new Recycle blocks pavement

This analysis focuses mainly on two of the SVAT models in ENVI-met [63]: in fact, the pavement layer with its effect is the main part of the system to be investigated, and it belongs to the Soil model. The use of simulations allows to investigate its behaviour in relation to the Atmosphere model. For this last reason the parameters relating to Vegetation and Transport models have been unchanged between the case study RS and the case study AS to clearly highlight how the pavement layer affects

the urban climate.

The Soil model in the simulation tool can belong to two different categories: the artificial (or waterproof) one, described by fixed parameters (albedo, emissivity, conductivity, mass, etc.), and the natural one, which considers also the heat exchange due to the mass transfer of water and humidity. The water content in the soil heavily affects heat transmission with the soil layers closest to the atmosphere. Impermeable surfaces fully convert energy into sensible heat, while in case of natural surface the water or humidity on the ground involves the conversion of a portion of the incoming energy into latent heat. Furthermore, both the thermal conductivity of the soil and its thermal capacity are directly related to the water content. This results in a reduced capacity for the dry soil to disperse heat towards the deeper layers. Finally, with reference to the absorbed radiation by the soil, ENVI-met tool considers the relationship between soil albedo, soil water content and solar zenith angle, according to the studies of Idso et al. [67]. They found that the albedo is influenced by both the moisture level in the soil and the angle at which sunlight strikes the surface. The albedo is a linear function of the water content in the uppermost soil layers. As soil moisture increased, albedo decreased, meaning wetter soils reflected less sunlight. Moreover, the albedo measurements are affected by the solar zenith angle, so to isolate the effect of soil moisture on albedo, it was necessary to account for and remove the influence of varying zenith angles. This adjustment allowed for a clearer understanding of how soil moisture alone impacts albedo.

Considering the properties of the Recycled blocks, this type of layer and relative surface has been assimilated to a natural one in the modelling process. A new surface objective has been added to the ENVI-met database as a soil with 20 % vacuum index and permeability of $3.27 \cdot 10^{-3}$ m/s. The soil model has been described with the following stratigraphy: the external layer as Recycled block of 8 cm and then the deepest layers as 35 cm of sand and simple gravel ground.

To evaluate the microclimate in urban areas, the simulation tool ENVI-met uses a set of equations to define the energy flows involved in the global energy balance, in order to evaluate the resulting temperature. A brief description of the equations involved in the simulation process is summarized below with reference to the study by Huttner [68]. The aim is to clarify how energy balances are defined and what quantities are involved in the calculation.

The energy balance between soil and atmosphere is solved at ground level by the Equation (2):

$$Q_{sw.net} + \varepsilon(Q_{lw.net} - \sigma T^4) - H - LE - G = 0 \quad (2)$$

where:

$Q_{sw.net}$ = net shortwave radiant energy flow, [W/m²].

ε = emissivity, [-].

$Q_{lw.net}$ = net longwave radiant energy flow, [W/m²].

σ = Stefan-Boltzmann constant, [W/m²K⁴].

T = thermodynamic temperature, [K].

H = sensible heat flow transmitted into the atmosphere, [W/m²].

LE = latent heat flow transmitted into the atmosphere, [W/m²].

G = heat flow transmitted to the soil, [W/m²].

The shortwave radiant energy flow $Q_{sw.net}$ is considered as incident solar radiation, given by the angle of incidence of the incoming shortwave radiation relative to the surface, the diffuse longwave radiant energy flow and the albedo. In this case the albedo is assumed as constant for the impermeable soil and in function of solar height, soil moisture and water content of the saturated soil for the natural soil, as discussed before in the text.

All bodies able to emit electromagnetic energy due to own temperature contribute to the calculation of longwave radiant energy flow $Q_{lw.net}$. The global balance of long-wave radiant energy flow therefore does not consider only the electromagnetic energy emitted by the soil, but also it considers the energy emitted by the foliage or walls of buildings.

About sensible H and latent heat LE flows transmitted into the atmosphere, energy depends on the humidity and temperature of the soil and on those of the lower atmospheric layer. In this case the Atmospheric model aims to realistically describe mass and energy exchanges in the urban boundary layer, taking into account local turbulent phenomena due to vegetation and buildings envelope. The turbulent fluxes H and LE are a function of the turbulent exchange coefficients and the temperature, the respectively humidity of the ground surface and the lowest atmospheric grid cell, according to the studies by Ali-Toudert [69].

In the calculation of the vertical heat flow transmitted to the soil G the parameter of thermal diffusivity in the soil λ_s is assumed as constant for artificial soils and function of the volumetric content of water for natural ones.

The simulation test has been developed by modelling different kinds of scenario with the aim to show how a specific porous block could mitigate the UHI effect: the reference layout (i.e. the RS case study) considers the current pavement made of standard and black cement blocks, while the investigated new layout (i.e. the AS case study) uses the Recycled blocks in substitution of actual pavement. In particular, the research focuses on the application of porous blocks in the parking area in front of the LabSCo Laboratory of Strength of Materials of IUAV University of Venice (pictures of the area are reported in the previous Fig. 3 and Fig. 4).

In Fig. 9 the simulation focus is pointed up: the pavement of the parking area interested in the replacement of the existing flooring with the Recycled light block (RLB) is highlighted with red cells as developed in the ENVI-met model, while a couple of receptors (#1, #2) are indicated in the picture to discuss hereafter in the text the temperature trends during the day. The term receptor is understood as a virtual probe; in practice, in the ENVI-met model, some virtual sensors have been placed to get the temperature values resulting from the simulation. The receptor #1 is chosen due to the position in the parking area, practically coinciding with the same position of the samples for the experimental test while the #2 is placed on the centre of area to evaluate appoint without obstructions and provide an average indication of the behaviour of the porous block in an empty impermeable area.

As aforementioned the soil and the pavement of the study area have been modelled according to Envi-met database. With reference to the in Fig. 9, the soil corresponds to the roadways around the study pavement depicted with the red grid. It consists of a 25 cm layer of road asphalt (characterized by 0.06 albedo and 0.94 emissivity) resting directly on the soil loam.

The pavement in the red grid, which represents the study object, is modelled according to the assessment scenario. For the RS scenario, the surface layer is composed of concrete blocks (characterized by albedo 0.13 and emissivity 0.87) forming a 35 cm layer, followed by a 15 cm layer of sandy soil and then the loam. The same RS stratigraphy is adopted for the AS scenario, with the substitution of cement for the RLB block, utilizing the properties obtained from laboratory characterization (albedo 0.31 and emissivity 0.93).

3. Results and discussions

This section of the paper reports and analysed individually the outcomes of the experimental tests and the numerical simulations, giving the priority to the experimental part having to characterize the product subsequently used in the simulation part. The final part presents a comparison between experimental and numerical test.

3.1. Experimental results

Following a thorough analysis of the thermal properties obtained from the laboratory tests, the next subsection delineates the field experiment results carried out on the three mock-ups, focusing on the temperature trend and on the heat flux through the samples and their surfaces. In addition, a statistical analysis has been included in this section to highlight the validity of the monitored data.

The subsection begins with the presentation of the climatic reference context, which is intended to support the ensuing discussion of the results obtained and to determine the heat flux calculation. Fig. 10 depicts the air temperature, the relative humidity and the solar radiation, which were recorded by the meteorological station (which have been used for the analysis); additionally, it illustrates the temperature measured on

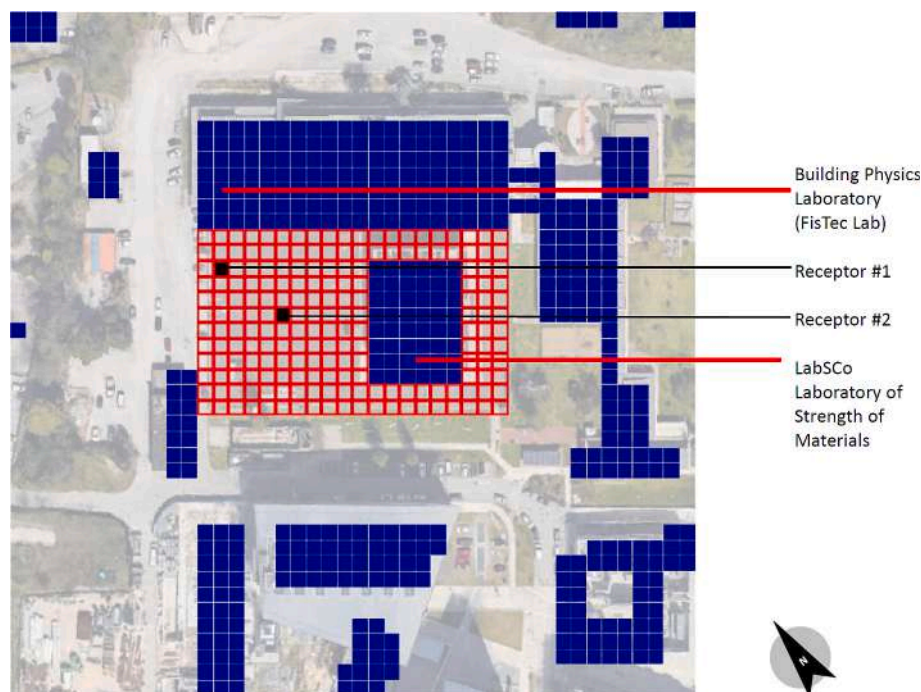


Fig. 9. Plan view of the numerical model with in red the analysis grid of the parking area, in blue the buildings and in black the location of two selected receptors. (For interpretation of the references to colour in this figure legend, the reader is referred to the web version of this article.)

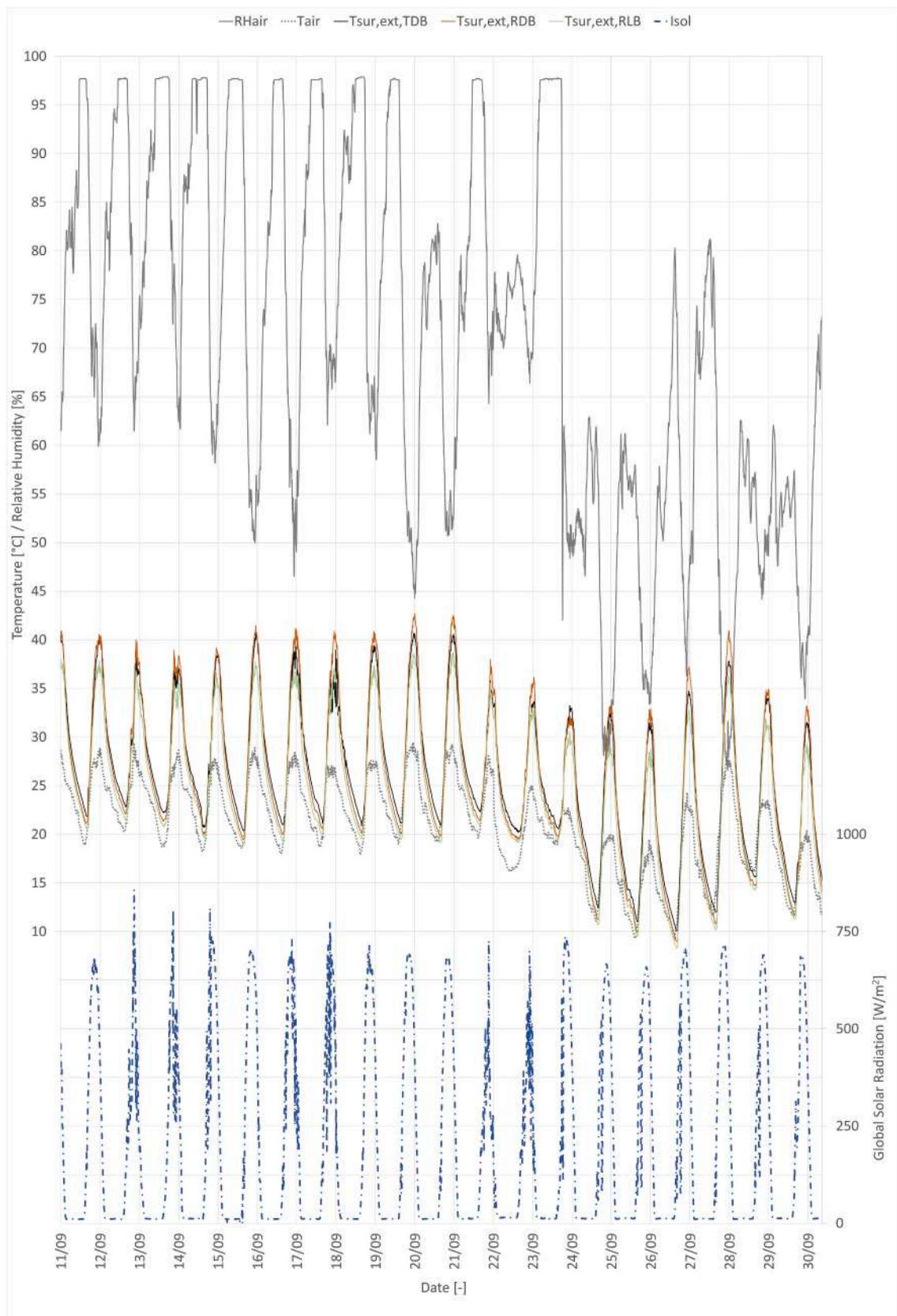


Fig. 10. Surface temperature of the pavements during monitoring period and climate data monitored by station of the Laboratory of Environmental and Building Physics of the IUAV University of Venice, for Air Temperature, Relative Humidity and Global Solar Radiation.

the external surfaces of the mock-ups during the monitoring period. These data address the subsequent description and discussion of the results.

Specifically, the analysis is conducted over the entire monitoring period, focusing on the representative day indicated (20/09) and on the warmest day (28/09) respectively. In these days the following data has been investigated: average, minimum and maximum temperatures, heat fluxes, thermal lag and time shift, with reference to the sensors placed in the mock-ups, as previously described in Fig. 7.

According to the charts in Fig. 10, the monitored period shows very similar daily trends in environmental parameters from 11/09 to 22/09, while in the last part of this period the temperature and relative humidity are quite different; on the other hand, the global radiation has a similar shape and intensity for the whole period. In the first part, the temperature varies from a maximum of 29 °C to a minimum of around 18 °C, while the humidity varies from 95 % to 47 %. In the following period, from 23/09 to 01/10, the average temperatures fall rapidly, even recording a gap of 10 degrees between the maximum temperatures of two consecutive days; 26/09 is the coldest day, the daily minimum temperature is 9 °C, while the maximum is 19 °C. Day 28/09 is the only one in this period that returns similar to the days of the first period, the maximum temperature was 29 °C and the minimum drops to 16 °C. The same trend is observed for relative humidity, with a range between 57 % and 37 %.

In Fig. 10 a same behaviour depending on the external temperature and solar radiation is observed on the surface temperatures of the three pavements and the values are comparable along the days with significant difference in terms of peak temperature, thermal attenuation in the inner layers and time shift. The thermal profile of the three blocks varies significantly during the diurnal cycle, as does the general thermal behavior of the materials (both heavy and permeable): during the morning hours, the material exhibits a propensity to absorb and retain heat; at noon, it undergoes a release of stored heat; in the afternoon, particularly on west-facing surfaces, there is a possibility of heat absorption; at night, the material releases heat to the environment. A discussion of this phenomenon must be undertaken in relation to the measurement data.

These behaviours are later discussed in relation to the measurement data because at first analysis the thermal behaviours appear homogeneous.

As mentioned above, the ANOVA analysis is proposed to understand if there are any significant differences that cannot be perceived in the first instance between the measured temperature values over the monitoring period.

According with the ANOVA analysis, F and P values for each group have been calculated: the larger the F-statistic is, the greater the difference in means between groups relative to the within-group difference, and for the P-value, if it is less than a pre-determined level of significance (fixed at 0.05), the null hypothesis is not valid and at least two of the groups are considered to be significantly different in their means [70].

A one-way analysis of variance (ANOVA) was conducted on the hourly temperature values measured in the three blocks throughout the monitoring period. The results of the analysis indicated a statistically significant difference between the three groups regarding temperature fluctuation, as evidenced by a value of $F > F_{critical}$ ($45.93 > 3.00$) and a $P\text{-value} < 0.05$.

Conversely, the analysis of the daily mean values from the three blocks revealed that the value of F was less than F critical ($1.23 < 3.17$) and the P-value (0.30) was greater than 0.05, indicating that there was no statistically significant difference between the three groups at the 5 % level of significance. This finding of Anova analysis suggests that the trend of daily mean temperatures does not exhibit significant differences. The observation that RLB exhibited a mean temperature of 24.14 °C was found to be approximately 1.5–2 °C lower than that of RDB (25.82 °C) and TDB (25.69 °C). However, this difference did not

significantly impact the minimal variability observed among the groups.

However, the analysis of the daily behavior yielded far more compelling insights.

Considering the experimental tests, with reference to the preview of the temperature trend shown in Fig. 10, the maximum surfaces temperatures plot in Fig. 11 show how the behaviour of porous samples (i.e. RLB and RDB) is different in comparison to the TDB: lower for RLB and higher for the RDB, with a maximum range of more than 3 °C respectively on 16/09 and 28/09 (as highlighted by the blue arrows in Fig. 11).

More specifically, the maximum and minimum temperatures during the entire monitoring period are reported in Table 7. As it can be seen, minimum and maximum temperatures in the RLB case are the lowest at each level of the sample; in addition, the RLB shows a range temperature between 1 °C and 4 °C lower compared to the two dark block ones (i.e. TDB and RDB). The maximum temperatures of the dark block are always higher at all levels than in the other samples; it is interesting that the minimum temperature recorded for each level is very similar to the TDB, indeed the minimum of the surface level is lower than TDB case. In the deeper layers of the three samples, the difference between the maximum temperatures of the samples decreases, while the minimum temperatures are very similar.

It is relevant to document the temporal occurrence and range of these minimum and maximum values during the monitoring period. As illustrated in Table 7, the maximum temperatures were consistently recorded on the external surfaces of the three blocks in the afternoon (approximately h 15:00), while the minimum temperatures were recorded in the morning (approximately h 8:00). These data occur on September 20th (or September 21st for RDB) and September 27th, respectively, but the trend also occurs on the other days surveyed. Specifically, the daily maximum values always occur in the afternoon (between h. 12:40 and 16:20) and the minimum values tend to occur in the morning (between h. 6:00 and 7:40).

In this regard, a one-way ANOVA analysis was performed under the assumption that there is not a significant difference in the thermal behavior of the blocks during the day and to assess that the observed differences are not due to random variations. A pair of sub-datasets of values were adopted, taking into account the time at which the maximum and minimum temperatures for the three blocks during each day of the monitoring period on the external surface were recorded, respectively.

The maximum temperatures occur, on average, between h 14:30 and h 15:00. The F-value ($2.90 < 3.17$) and P-value ($0.06 > 0.05$) indicate that there is no statistically significant difference between the three groups at the 5 % level of significance. However, the P-value suggests the presence of a potentially noteworthy trend, particularly between TDB and RLB, which might have become more apparent with a larger sample size and an expanded number of days observed.

The minimum temperatures are observed to occur on average at h. 8:00, and the F-value (0.01) is found to be significantly lower than the critical value (3.17). Additionally, the P-value (0.98) is determined to be substantially greater than 0.05, indicating that there are no substantial differences between the groups with respect to the time of minimum temperature. The findings indicate that the type of block (standard or recycled, dark/light) does not influence the recorded minimum temperature. The observation at h. 23:40 in all three groups may appear anomalous, but it does not alter the overall conclusion, as it occurs identically in each group.

The analysis of variance (ANOVA) was also repeated for the data of the other levels in the mockups (described on Fig. 7).

The same statistical considerations can also be applied to the internal surface temperatures of the blocks. The maximum temperatures are observed to occur around h. 16:30, the F-value (0.82) is less than critical (3.17). The P-value (0.45) is greater than 0.05. The minimum temperatures are observed to occur around h. 8:10, the F-value (0.01) is less than critical F (3.17), and a P-value (0.99) is much greater than 0.05.

At the –10 cm level, the situation undergoes a notable shift, and the



Fig. 11. Maximum temperature on external surfaces of the specimens during the monitoring period.

Table 7

Maximum and minimum value of temperature recorded in the 4 layers during monitoring period (date and time of the recording are shown in brackets).

Temperature [°C]	External surface of the block	Internal surface of the block	-10 cm	-25 cm
T,max TDB	40.7 (20/9/18, h 15:10)	37.4 (20/9/18, h 16:30)	30.9 (12/9/18, h 19:40)	29.5 (12/9/18, h 23:50)
T,min TDB	10.1 (27/9/18, h 7:40)	11.4 (27/9/18, h 8:20)	16.0 (27/9/18, h 11:00)	16.6 (27/9/18, h 13:00)
T,max RDB	42.7 (20/9/18, h 15:40)	38.2 (20/9/18, h 16:30)	32.3 (12/9/18, h 18:50)	30.1 (12/9/18, h 00:00)
T,min RDB	9.0 (27/9/18, h 7:20)	11.5 (27/9/18, h 8:20)	16.1 (27/9/18, h 10:30)	18.1 (27/9/18, h 14:20)
T,max RLB	38.7 (21/9/18, h 15:10)	33.7 (21/9/18, h 16:50)	28.7 (12/9/18, h 20:40)	28.0 (12/9/18, h 01:00)
T,min RLB	8.3 (27/9/18, h 7:10)	10.3 (27/9/18, h 8:20)	15.2 (27/9/18, h 11:40)	16.5 (27/9/18, h 14:30)

time of maximum temperature changes significantly among the three groups. The maximum temperatures are observed during nocturnal hours, specifically between h. 18:40 and 23:50. It is noteworthy that the RDB tends to record maximum temperatures at least one hour earlier than the TDB and RLB. The times at which maximum temperatures are recorded are more frequent around h. 7 for the TDB and RDB, while for the RLB, it is more frequent around h. 23:50. A statistically significant difference is observed, as evidenced by the F-value (4.94) is higher than the critical value (3.17), and a P-value of 0.01 is lower by 0.05. On the other hand, minimum temperatures occur in the morning on average between h. 10:20 and 12:00, and a F-value of 3.07 is lower than the critical F = 3.17, and a P-value of 0.01 is lower by 0.05.

Finally, even at the -25 cm level, there is a statistically significant difference in temperature between the three groups, with changes in both maximum and minimum values. The F values (4.40 max, 5.84 min) are higher than the critical F value (3.17), and the P-values are less than 0.05.

Therefore, going deep into the mockup levels, the analysis reveals substantial disparities between the means of the maximum and

minimum values identified. This discrepancy is likely attributable to the fact that the ANOVA assumes normality of the distributions within groups. However, the dataset consists of only a limited number of days/observations per group, with a high frequency of repeated values (e.g., h 23:50 repeated six out of nineteen in one group). Consequently, the data does not appear to be normally distributed.

The statistical analysis reveals a consistent pattern in the relationship between the maximum and minimum temperatures detected in RLB and the time offset from TDB and RDB.

In addition, it is possible to express some observations regarding aspects related to the thermal inertia of the specimens. The inertia represents the ability of a material to change its temperature more or less slowly in response to changes in external temperature or a heat source. The daily range temperature (difference between maximum and minimum temperature values), recorded on the external layer of the blocks, shown in Table 8 appears to be similar for TDB and RLB (almost 26 °C), while it is 4 °C higher for RDB. In the internal layer, instead, the RLB shows a difference of 17.6 °C, about 4 °C lower than RDB and 2 °C lower than TDB. The values of maximum daily range of temperature have been recorded on 28/09 as better discussed hereafter in the text of the paper.

The surface temperature and behaviour of the three samples can be analysed more in detail considering a whole day. In Fig. 12 the measured values for the 20/09 are shown because it represents the day with the maximum outdoor air temperature, equal to 29.5 °C that occurred during the monitoring period.

The resulting surface temperatures are significantly affected by heat fluxes exchanged with the surroundings area and global solar radiation. The latter normally increases the surface temperature depending on the time of day. As it can be seen in the chart, during the day, global solar radiation rises to a peak at midday, in the period between 11:00 and 13:00 and then slowly decreases, but the radiative balance of surfaces keeps positive for a few hours. This means that solar radiation provides the surfaces with more energy than that released by the specimen, which

Table 8

Max daily range in the 4 layers during monitoring period.

Daily Range of Temperature [°C]	External surface of the block	Internal surface of the block	-10 cm	-25 cm
TDB	25.8	19.6	6.5	4.6
RDB	30.1	21.4	7.2	3.6
RLB	26.1	17.6	5.0	3.1

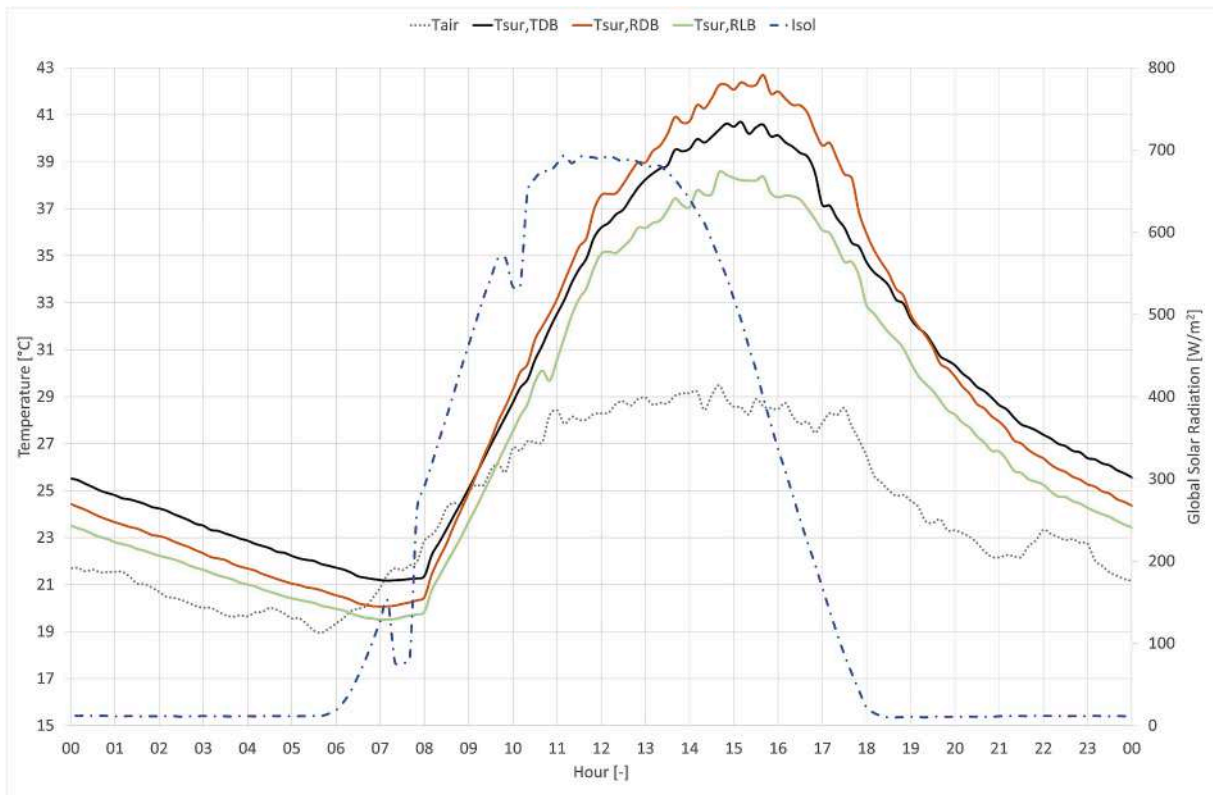


Fig. 12. Temperature on the external surfaces of the specimens and global solar radiation on 20/09.

thus continues to warm up. As a result, the air temperature near the surface also continues to increase until 16:00, until the surface radiative balance reaches the equilibrium.

Comparing the three specimens, the surface temperature of the RLB is always lower during all hours of the day; the RDB, on the other hand, maintains higher temperatures than the TDB during the day, but shows

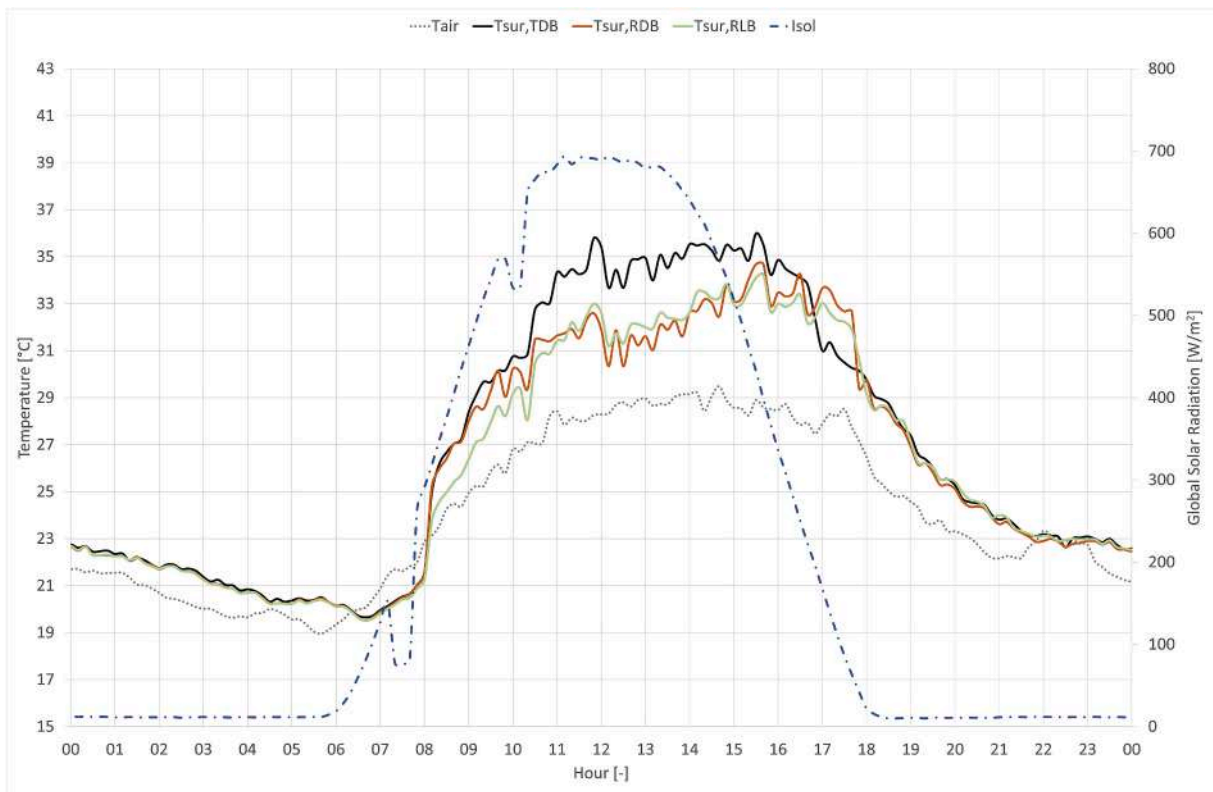


Fig. 13. Air temperature at height + 10 cm from external surface of each sample on 20/09.

levels of attenuation from dusk to dawn such that temperatures are lower, probably due to the porous structure of the material.

On the other hand, the air temperature measured at a height +10 cm from the surface of each sample is quite different. The trends of the air temperature at this measure point are reported in Fig. 13.

For the cases RLB and RDB, the temperatures follow a similar trend, but with a lower incidence; the values are even more than 2 °C lower in the RLB case study; the temperature continues to increase gradually, reaching its peak in the afternoon at 16:00; this behaviour highlights an heat wave only at the end of the afternoon from 16:00 to 18:00 which corresponds to the period of the day when the temperatures of the RLB and RDB are higher than TDB.

The charts in Fig. 14, Fig. 15, Fig. 16, describe the temperature trend measured on 20/09 in the different layers of each sample (TDB, RDB and RLB), focusing the time and the value of maximum and minimum temperatures by coloured markers. The maximum temperature of the TDB in the outer surface layer is 40.7 °C, decreasing by 3.3 °C to the inner surface layer of the block (37.4 °C), while at depths of the sample of 10 cm and 25 cm the temperature decreases to around 31–29 °C (see Fig. 13). For the other two samples, the difference between the two first layers is greater, with the temperature decreasing by approximately 1.2–1.6 °C; the range is 4.5 °C for the RDB (see Fig. 15) and 4.9 °C for the RLB (see Fig. 16).

Table 9 summarized the values recorded on 20/09 and discussed before in the text. A focus can be assessed on the thermal gradient, i.e. the ratio of the temperature difference between the surfaces and the thickness of each block (equal to 8 cm). The TDB and RLB have a similar temperature trend and temperature difference between #1 and #4 layers (11.5 °C), while the temperature difference between the surface of the element (layer #1 and #2) is respectively 3.3 °C and 4.9 °C, so the value of thermal gradient is greater for the RLB (60.9 °C/m) than for the TDB (41.1 °C/m). This result of to the thermal properties of the two materials, precisely because it has a lower thermal conductivity for the same thickness (see thermal conductivity values in the Table 4).

According to the temperature measures on the four layers in each facility as shown in Fig. 14, Fig. 15 and Fig. 16 during the 20/09, a thermal delay along the day is determined with reference to the maximum solar radiation at 12:00. The delays are summarized in Fig. 17. The different samples reach the maximum temperature on the external surface with a delay of 2.39 h for light block, less than the other samples. On the internal surface a phase shift of around 4:30 h of delay is similar for the samples. The thermal lag and the time delay increases with depth in the last two layers, where the thermal lag is in favour of the light block.

A focus on trends and results given by the period 23/09 and 30/09 could be discussed due to the external environmental data of the meteorological station (mentioned in Fig. 10) and due to the recording of the max daily range of temperature mentioned above. In fact, the chart in Fig. 18 shows that in this period the daily range of temperature presents a different behaviour due to the meteorological variations in cloudiness and temperature during the days, resulting in maximum values of daily range on 28/09, as, for each level.

The chart in Fig. 19 describes how the solar radiation and the outdoor temperature decrease until day 26/09, so the surface temperatures of the samples are also lower than during the month, then until day 28/09 the outdoor temperature increases rapidly.

Fig. 20 depicts the surface temperatures difference between the three samples, comparing pairwise profiles during the monitoring period. A comparison of TDB and RLB data reveals that TDB temperatures are consistently higher, with a mean difference of approximately 4 degrees on 24-25-26/09. During early morning hours, at 8:00, the temperature differences are minimal (approximately 1 °C); then the temperature difference rises till 16:00 and subsequently decreases until the early hours of the next day. In contrast, the temperature variations between TDB and RDB exhibit a more recurrent and customary pattern over the course of the day. During daylight hours, which extend from 9:00 to 18:00, the surface temperatures recorded at RDB are elevated, with a maximum disparity of approximately 2 °C. Conversely, during nocturnal

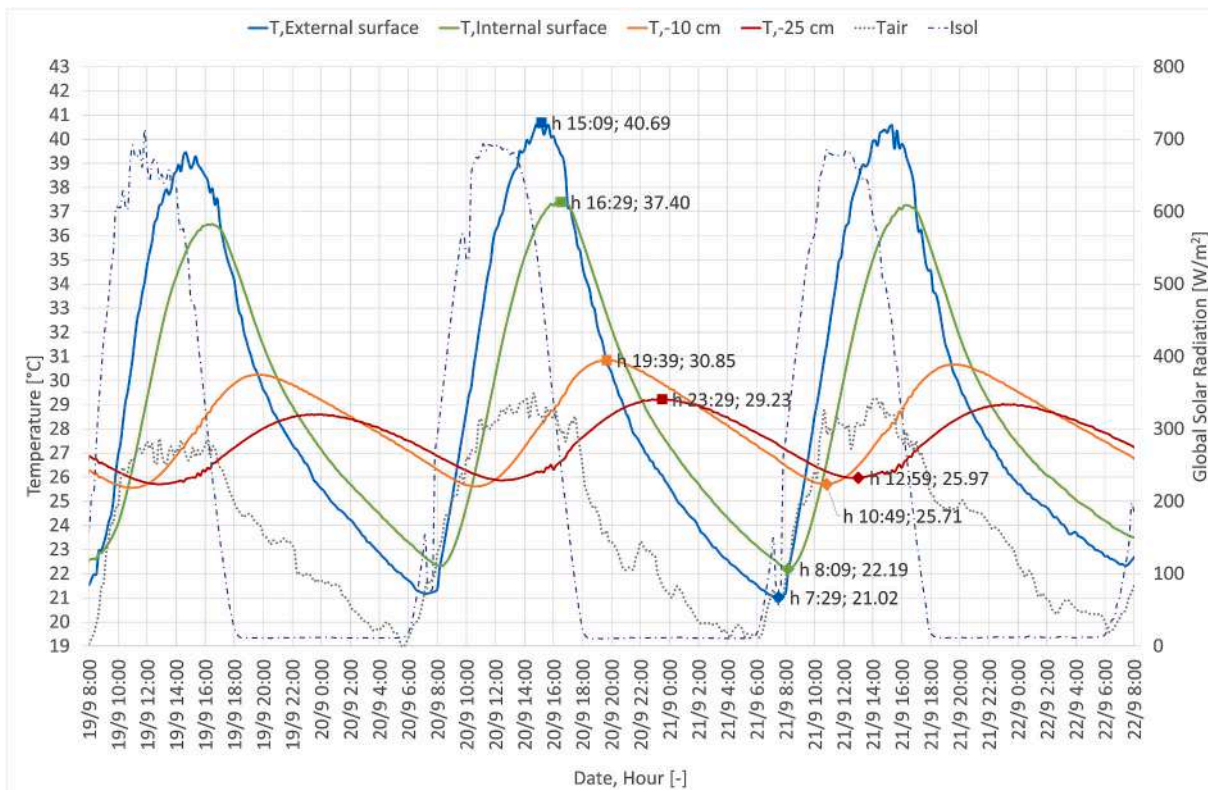


Fig. 14. Temperature trend for TDB, focus on 20/09.

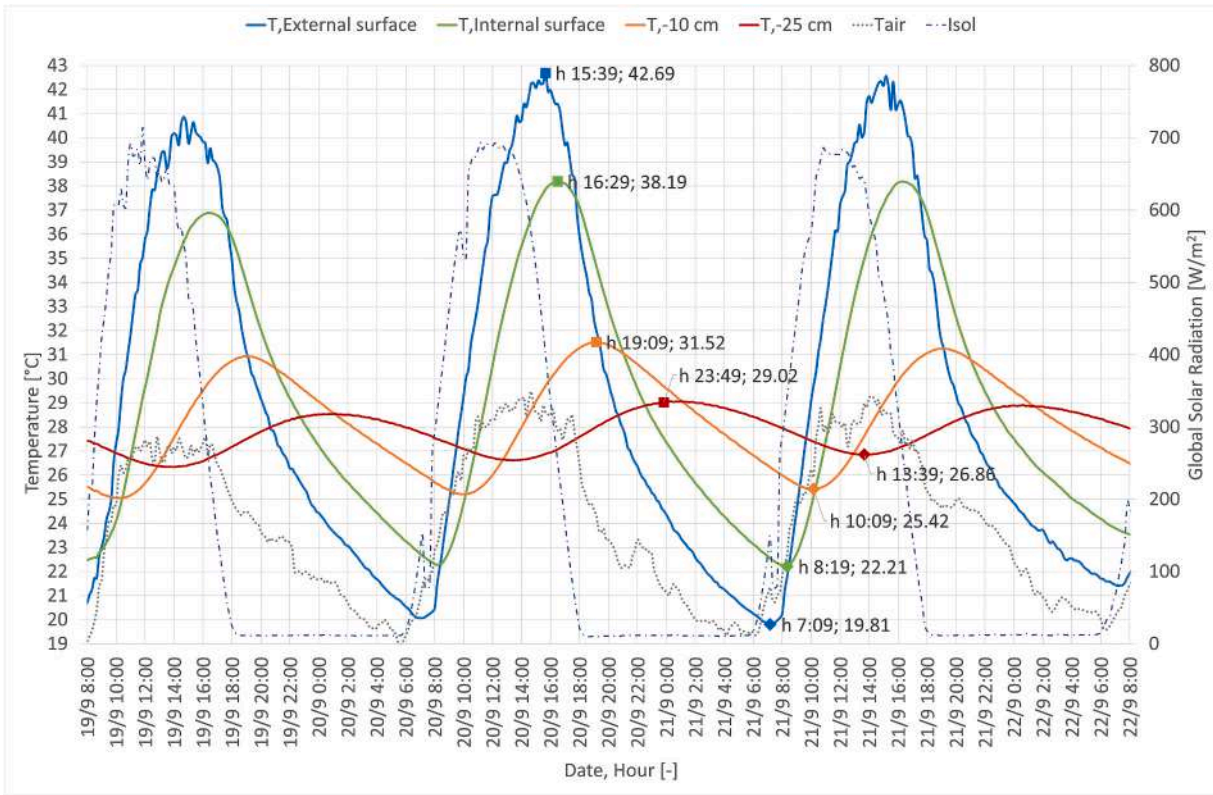


Fig. 15. Temperature trend for RDB, focus on 20/09.

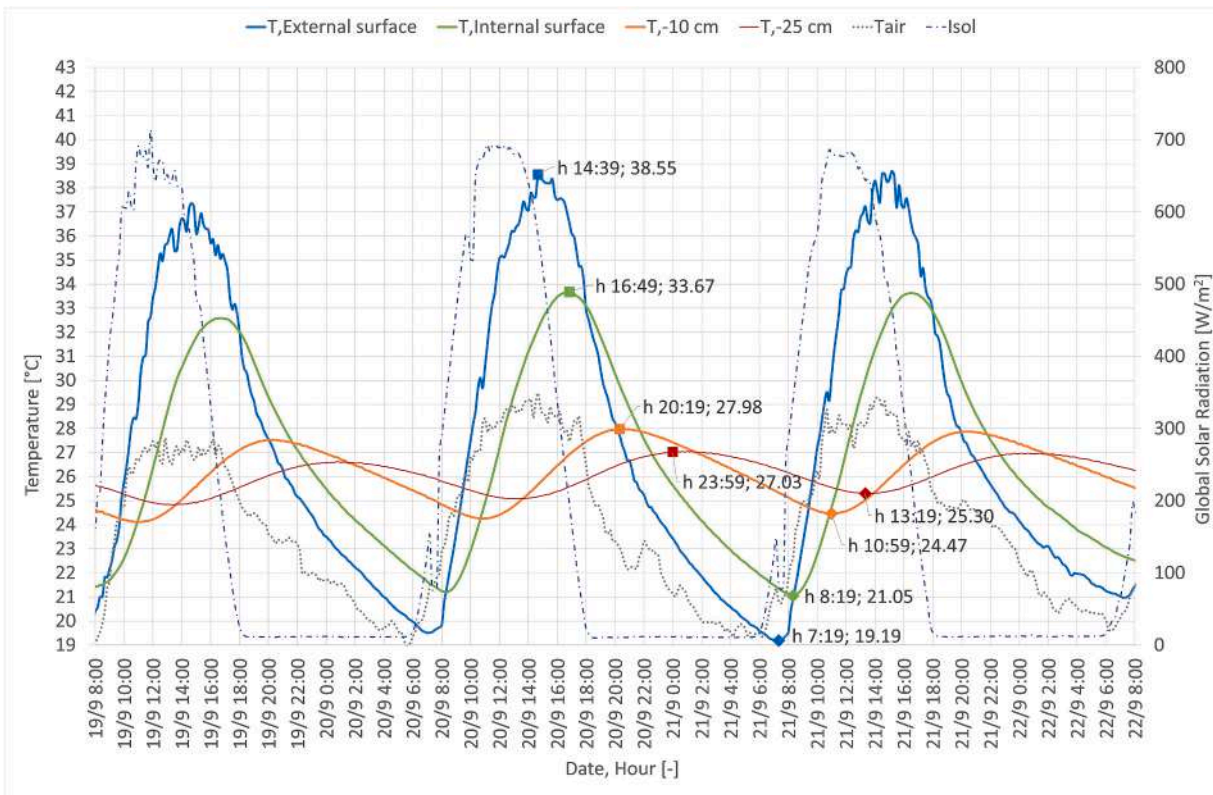


Fig. 16. Temperature trend for RLB, focus on 20/09.

Table 9

Temperature trend between the layers of the samples and temperature gradient of the three blocks on 20/09.

	#1 layer, External surface [°C]	#2 layer, Internal surface [°C]	Range #1-#2 [°C]	#3 layer, -10 cm [°C]	Range #2-#3 [°C]	#4 layer, -25 cm [°C]	Range #3-#4 [°C]	Range #1-#4 [°C]	Temperature gradient Tg #1- #2 [°C/m]
TDB	40.7	37.4	3.3	30.8	6.6	29.2	1.6	11.5	41.1
RDB	42.7	38.2	4.5	31.5	6.7	29.0	2.5	13.7	56.3
RLB	38.5	33.7	4.9	28.0	5.7	27	1.0	11.5	60.9

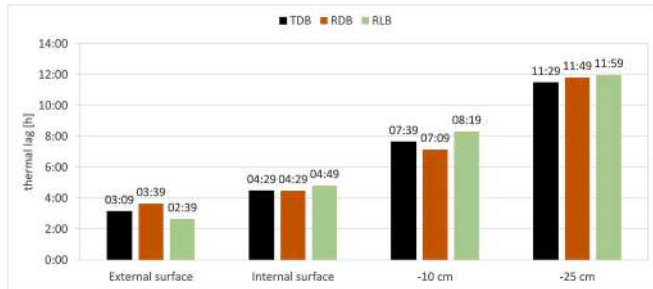


Fig. 17. Analysis of the thermal lag starting from the maximum solar radiation at 12:00 on 20/09.

periods, the trend is reversed, and the TDB temperature is augmented, with a consistent gap of about 1 °C for the majority of hours (from 22:00 to 7:00). The temperature difference profile between RLB and RDB is analogous. Despite their identical material composition, the two blocks exhibit substantial temperature differences, probably due to the different values of α_s and SRI_{avg} reported in Table 5. During the morning period (from 6:00 to 14:00), the temperature difference escalates rapidly, with peak differences of at least 3–4 °C; the trend is repeated backwards in the afternoon-evening hours, then during the difference is approximately 0.5–1 °C, and subsequently diminishes gradually until the following morning.

Finally, the thermal behaviour of the material is discussed by presenting the data monitored during the different periods of the day (late night, early morning, morning, early afternoon, afternoon, evening, night).

The Fig. 21 shows the average temperature values of the external surfaces of the samples during the different periods; the data considered are for the period from day 12/09 till day 23/09, since it is more representative of the monitored period and is characterized by a similar trend.

It can be concluded that during the day, the RLB temperatures are always lower on average than the two samples, with maximum values about 2 °C lower than the TDB and almost 4 °C lower than the RDB, recorded in the afternoon. The temperatures of RDB are the highest of the other samples during the day, precisely from late morning until evening.

A comparison between the outcomes of the experimental tests is developed as follows. The attenuation and phase shift values given by the experimental temperature measurements on the mock-ups (reported in Fig. 14, Fig. 15, Fig. 16) are compared with those calculated using the thermal diffusivity data obtained from hot disk measurements (reported in Table 5). In this case the phase shift ϕ and attenuation A are calculated with the following Equations (3) and (4):

$$\phi = \beta L, [\text{rad}] \tag{3}$$

$$A = e^{-\beta L}, [-] \tag{4}$$

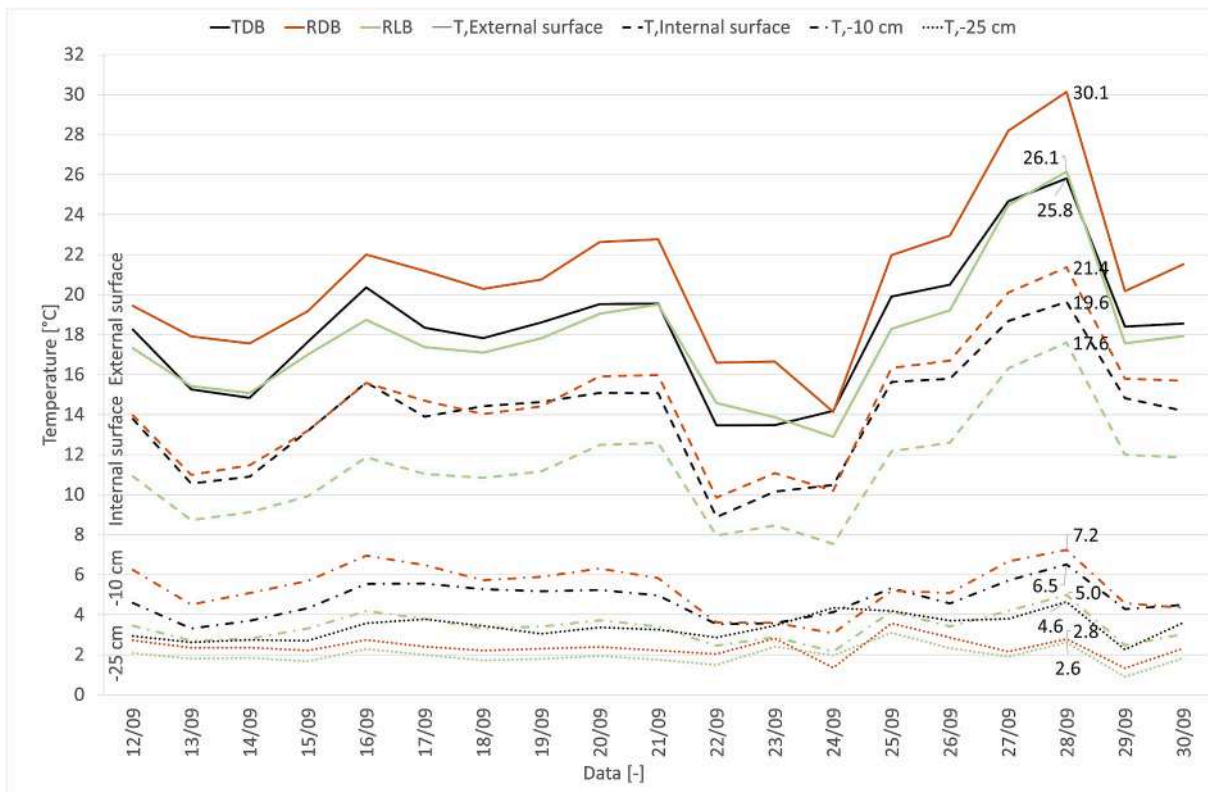


Fig. 18. Max daily range of temperature in the 4 layers during monitoring period for each sample.

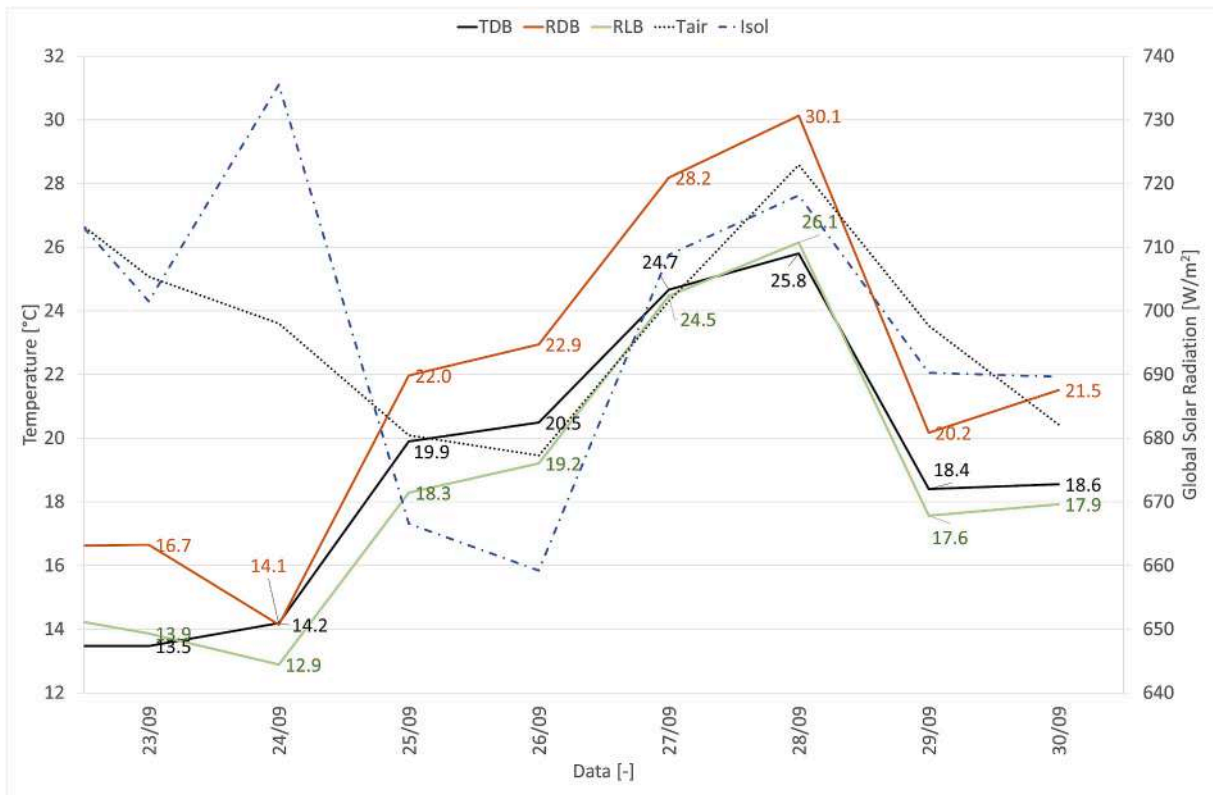


Fig. 19. Max values between 23 and 30/09 for solar radiation, temperature of outdoor air and temperature on external surface of each sample.

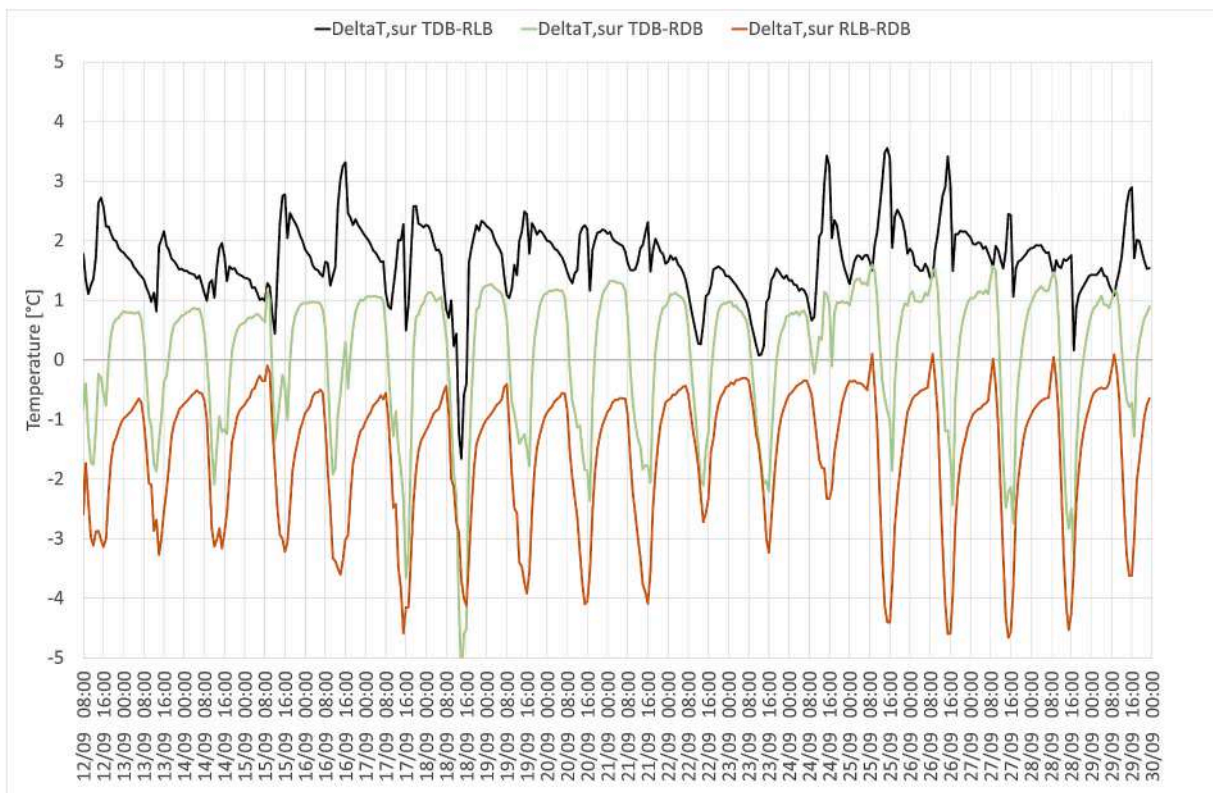


Fig. 20. Difference of temperature between the three samples, comparing pairwise profiles during monitoring period.

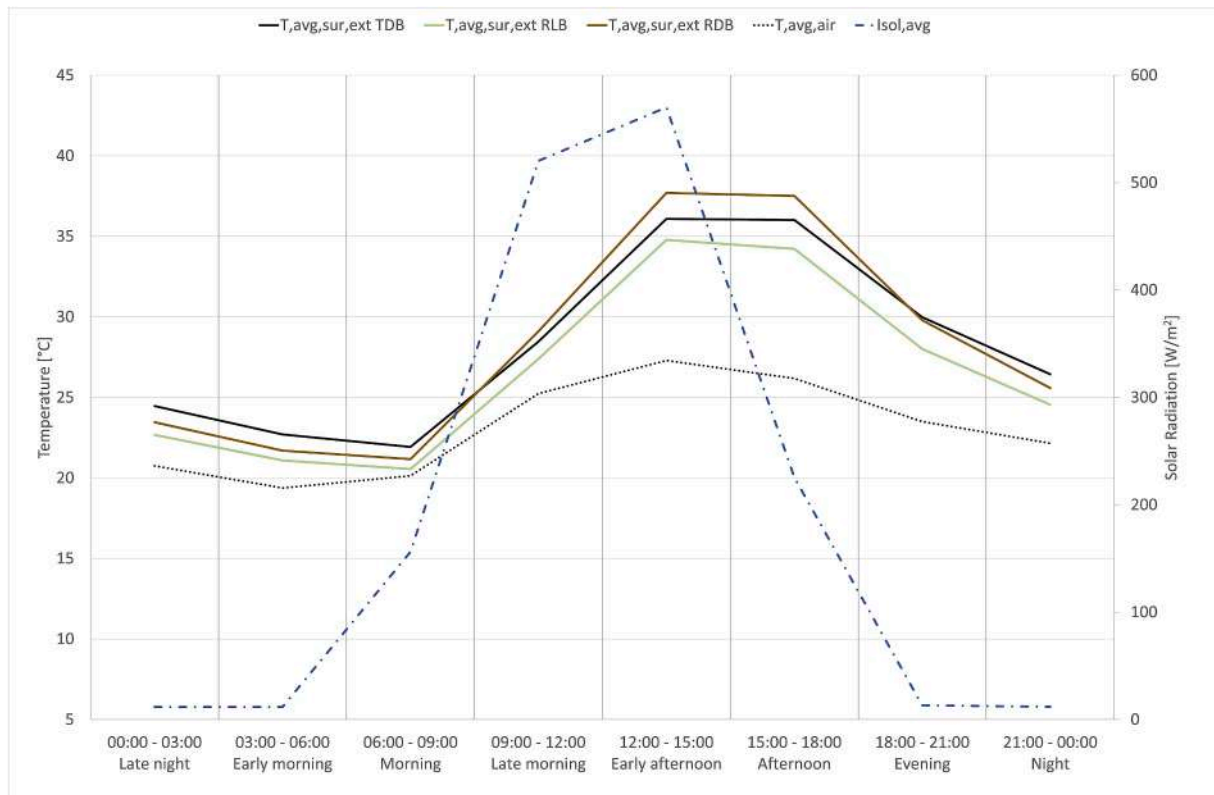


Fig. 21. Temperature values recorded on the external surfaces of the samples during the period from day 12/09 till day 23/09. The values have been calculated as average during the different periods of the day.

where:

$\beta = \sqrt{\frac{\pi f}{\alpha}}$ is the phase constant, given by the wave frequency f and the attenuation constant α .

L is the thickness of the specimen, [m].

Considering a frequency calculated over 24 h and the thickness of the sample TDB, the results are a phase shift $\phi = 0.42$ [rad] and an attenuation $A = 0.66$ [-]. According to the $\Delta t = \frac{\phi}{2\pi f}$, the thermal phase shift is calculated in hours, resulting in $\Delta T = 1:36$ [h].

Considering the temperature data given by the mock-ups, an average phase shift $\phi = 1:18$ [h] and an attenuation $A = 0.66$ [-] are calculated for 24-hour cycles over the 19 days of monitoring period (from 12/09/2018 to 30/09/2018) from temperature measurements on both the surfaces of the sample.

Finally The Table 10 reports and give a comparison of the results, showing a good match between the data calculated by both methods; the difference of phase shift is 0:18 [h], less than the values of standard deviation calculated in 0:23 [h], while the difference of attenuation is 0.07, slightly higher than the standard deviation calculated in 0.07 [-].

The thermal behaviour of the three specimens is given and compared, by considering the field measurements of the temperature and the climate parameters and thermal properties by laboratory test (solar absorptance, emissivity, thermal conductivity).

Table 10

Comparison the phase shift and attenuation values calculated with data from hot disk measurements and data from mockups monitoring.

	Phase shift [h]	Attenuation [-]
From calculation using diffusivity from hot disk measurements	1:36 (+0:18)	0.66 (-0.07)
From temperature data: Average	1:18	0.73
Standard deviation	0:23	0.03

The heat flux of the specimens is calculated considering the different energy contributions, including solar radiation (E_{rad}) and heat transfer by conduction through the specimen (E_{cond}) and exchanged by convection with the air (E_{conv}), according to the Equation (5a).

$$E = E_{rad} + E_{cond} + E_{conv} \tag{5a}$$

$$E_{rad} = E_{rad,day} + E_{rad,night} \tag{5b}$$

$$E_{rad,day} = \alpha_s \cdot I_{sol} \cdot S \cdot t \tag{5c}$$

$$E_{rad,night} = \varepsilon \cdot \sigma \cdot S \cdot (T_{air+10cm}^4 - T_{sky}^4) \cdot t \tag{5d}$$

$$E_{cond} = \frac{\lambda \cdot S \cdot (T_{sur,int} - T_{sur,ext})}{L} \cdot t \tag{5e}$$

$$E_{conv} = h_c \cdot S \cdot (T_{air+10cm} - T_{sur,ext}) \cdot t \tag{5f}$$

where:

E = Total Heat Flux, [MJ].

E_{rad} = Heat Flux Induced by Radiation, [MJ].

E_{cond} = Heat Flux Induced by Conduction, [MJ].

E_{conv} = Heat Flux Induced by Convection, [MJ].

S = Surface Area, [m²].

I_{sol} = Global Solar Radiation, [W/m²*K].

α_s = Solar Absorptance, [-].

ε = Emissivity, [%].

σ = Stefan-Boltzmann Constant, [W/m²*K⁴].

λ = Thermal Conductivity, [W/(m*K)].

t = Time, [s].

L = Thickness, [m].

T_{sky} = Sky Temperature, [°C].

T_{dp} = Dew Point Temperature, [°C], defined as $T_{sky} = T_{air+10cm} \cdot (1 - 0.31 \times e^{-0.13(T_{dp}-273.15)})$

h_c = Convection Coefficient, $[W/(m^2 \cdot K)]$, defined as

$$h_c = 5.6 + 4.0v \text{ for } v \leq 5.0 \text{ m/s}$$

$$h_c = 7.2v^{0.8} \text{ for } v > 5.0 \text{ m/s}$$

The heat flux induced by radiation is calculated considering the daily and night radiation, according to Equation (5b); the night radiation

considers the sky temperature (T_{sky}), calculated according to the formula di Berdahl and Fromberg [71], according to Equation (5d); the selection of this formula is predicated on its superior capacity to account for the effects of humidity with greater precision, a feat accomplished through the integration of dew point temperature (T_{dp}); this formula

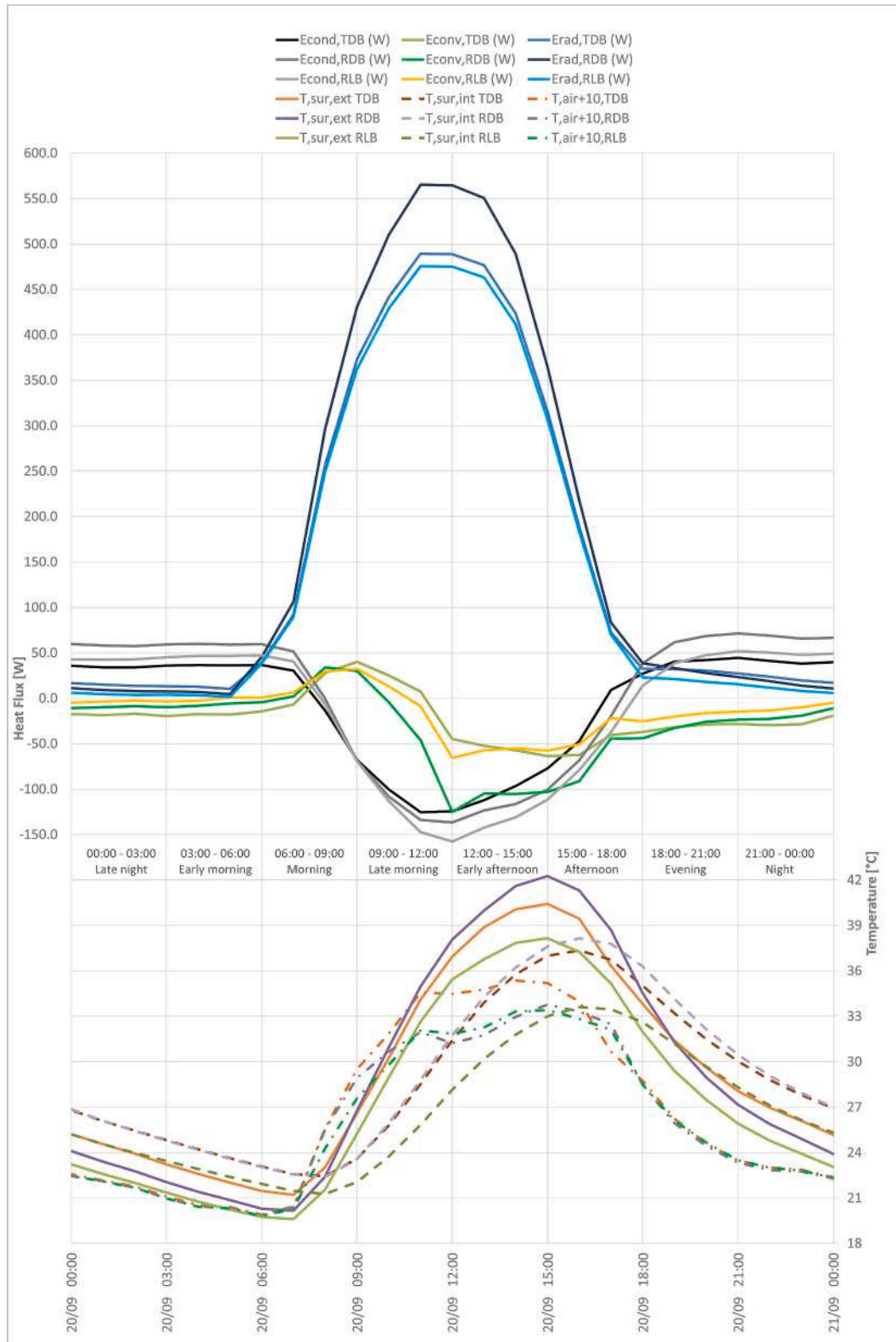


Fig. 22. Heat flux trend calculated for TDB-RDB-RLB, focus on 20/09, induced by radiation, conduction and convection, with reference to the measured temperatures on the external and internal surfaces of the specimen and outdoor at + 10 cm above the external surface.

exhibits enhanced performance in environments characterized by high relative humidity when compared to conventional methods that are predicated solely on the temperature of the air. The heat conduction E_{cond} is calculated according to the Fourier's law in Equation (5e). The heat flux induced by convection E_{conv} is calculated using Equation (5f) [72]. The calculation applied considers the external air temperature at +10 cm above the external surface of each specimen.

The charts in Fig. 22 describe the heat flux trend calculated for the specimens, focus on 20/09, induced by radiation, conduction and convection, with reference to the measured temperatures on the external and internal surfaces of the specimen and outdoor at +10 cm above the external surface. The analysis was carried out with a resistive calculation model, without considering the thermal capacity of the specimen.

In the charts, the heat absorbed by the samples is given a negative sign and heat emitted is given a positive sign. As can be seen from the figures, the heat flux is positive because it is more influenced by solar radiation, which is offset by conduction and convection absorption during daylight hours.

During the daytime, heat is transferred to the outside; the largest contribution is from solar radiation, which heats the air from 6:00 to 18:00 and flows outward; conversely, by conduction, it is absorbed by the sample with a slight delay, that is, between 8:00 and 17:00; by convection, the heat is absorbed by the warm air in the sample, except for the morning hours from about 7:00 to 11:00, when the temperature of the outside air is greater than or equal to that of the outside surface of the sample.

At night, the situation is reversed, the outdoor temperature falls below the indoor temperature, and the same happens in the two sample surfaces, so that the temperature of the indoor surface is greater than the outdoor surface from 18:00 the day before until 7:00 the next morning. Heat flows in the opposite direction: fluxes by radiation and convection

cancel each other out, and the total flux is influenced only by conduction. The flux by radiation is practically minimal due to the absence of solar radiation and the low contribution of the sky temperature; the heat absorbed by convection has a minimal contribution that decreases from 18:00 the day before to 7:00 the next morning as the temperature difference between the air and the outside surface decreases; likewise, the heat by conduction is transferred to the outside with constant values, since the temperature difference between the inside and the outside surface is constant.

3.2. Simulation results of the scenarios

By using the Leonardo module in ENVI-met, the results of the simulation activities on the two scenarios (RS and AS) are presented in two subsections: a first one describes the outcomes on an urban area larger than the intervention area, the second one focus in more detail on the surroundings of the intervention area, as shown in Fig. 9.

3.2.1. Results of the reference scenario RS

In the RS the microclimatic attitude reveals an evident contrast between the large waterproofed and paved surfaces (extremely warm) and the green areas. The parking area is covered by a specific kind of cement pavement, while the rest of the surrounding area is covered by an asphalt layer. The main characteristics adopted in the model are summarized in Table 6. This analysis shows surface temperatures among the highest in the case study area as shown in Fig. 23. In particular, during the day the surfaces temperatures in the parking area have a range between 36 °C and 56 °C. The nearby presence of the canal in the north-east and the green area extending from the south-east area are very significant but are unable to mitigate the microclimatic conditions.

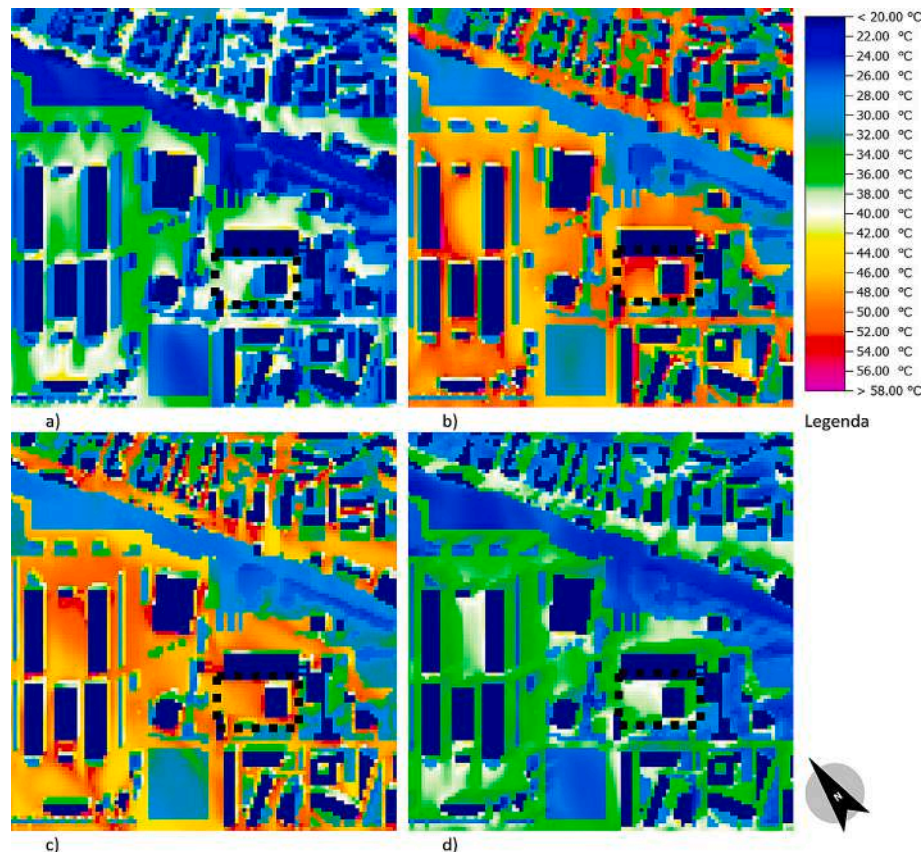


Fig. 23. Surface temperature of the RS scenario at a) h. 9, b) h. 12, c) h. 15 and d) h. 18 on 02/08; the box in black dash line in the figures defines the intervention area of the parking of the University.

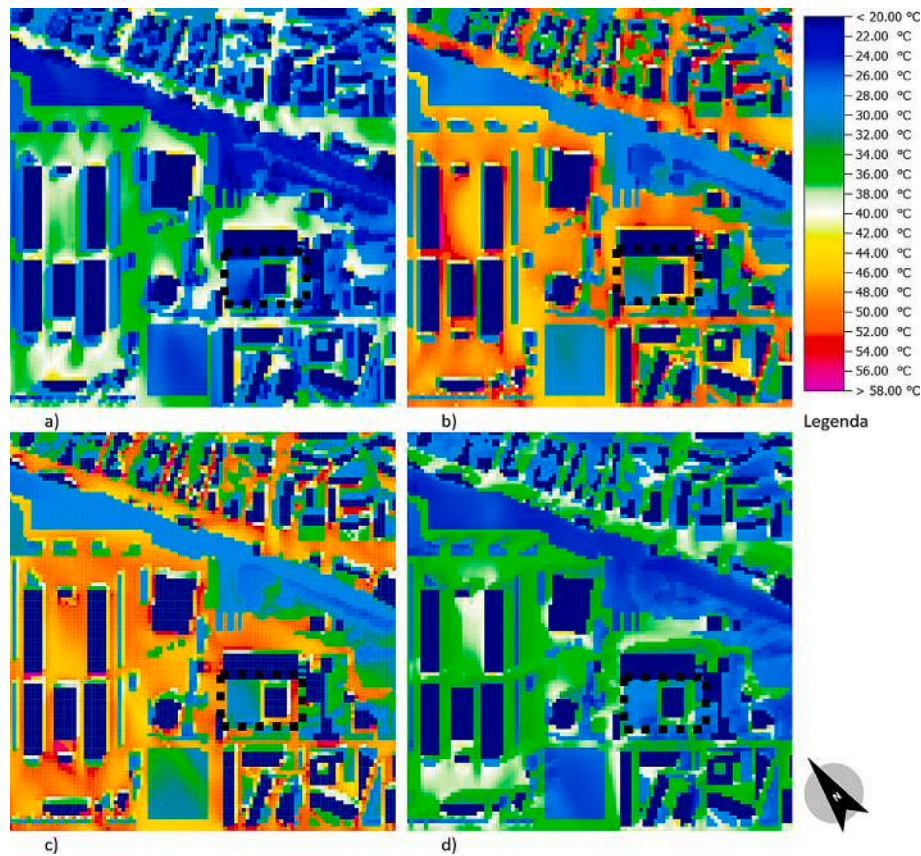


Fig. 24. Surface temperature of the AS scenario at a) h. 9, b) h. 12, c) h. 15 and d) h. 18 on 02/08; the box in black dash line in the figures defines the intervention area on the parking of the University District.

3.2.2. Results of the analysis scenario AS

In the AS the cement pavement is substituted with the light porous block. The Fig. 24 shows how in the parking area the surfaces temperatures are lower than in RS; during the day the values recorded a range between 22 °C and 38 °C. The application of the porous elements mitigates the microclimatic conditions only on the interested area and in a minor part along the boundaries, without significant impact on the nearby zone covered by asphalt.

3.2.3. Comparison between RS and AS

In AS the impact of porous pavement is remarkable from a microclimatic point of view. In the interested area, a significant latent heat flow determines a marked reduction in the surface temperature of the soil, that corresponds to a significant reduction in air temperature. The comparisons of latent heat flux and surface temperature, between RF and AS, are reported respectively in Fig. 25 and Fig. 26. Each figure reports the values of the variables in 4 different hours of the day. The following paragraphs discuss the trends of the environmental parameters during the daytime simulated.

Early in the morning, at 9:00, when the effects of solar radiation on the microclimate are still negligible, the performance of RLB in AS is similar to natural soil. During the day the latent heat and the resulting surface temperature are linked, and they must necessarily be discussed together. In fact, as can be seen in Fig. 25, in the parking area, a difference of about 200 W/m² in latent heat flow between the two scenarios is depicted. The increase of latent heat flux is due to the permeability of the material, this has led to a reduction in the surface temperature. As it can be seen in Fig. 26, the surface temperature is about 8 °C lower than in RF and consequently the air temperature at 1 m height is reduced by about 1.2 °C on average.

At midday, the situation undergoes a remarkable change. Solar

irradiation triggers important evaporation phenomena in the soil, bringing the latent heat flow even beyond 450 W/m², as shown in Fig. 25. In comparison with RS, the soil surface temperature is reduced by almost 20 °C (Fig. 26) the air temperature is reduced by 2.3 °C on average.

Even if the peak temperatures of the soil and the atmosphere are reached at 13:00, the climatic parameters of latent heat flux and surface temperature stay essentially on the same levels until 15:00, except for slight differences related to the solar path.

In the late afternoon at 18:00 the results are very similar to the early hours of the day, characterized by a latent heat flow of almost 200 W/m² (see Fig. 25). A difference in the surface temperature of about 10 °C (see Fig. 26) corresponds to a reduction in the air temperature of about 1.5 °C on average.

3.3. Comparison between experimental and numerical test

This section's intention is slightly different to the previous ones, and it wants to present the behaviour of the pavement obtained in the two modalities (experimental activities and numerical simulations), to confirm the similarities and differences during a hot day. Even though the days presented here are not the same for the experimental and simulations output data, they are typical days representative at local urban level. In fact, the choice of the hottest day for the numerical part falls on a day of August, a period not covered by the monitoring activities of the experimental tests. This day has been compared to the hottest day within the monitoring period of the experimental activity.

The results of experimental tests and numerical simulations are discussed in this section with reference to the temperature trends reported in Fig. 27. It is worth remembering that the comparison has been done starting from the same meteorological data gathered from the

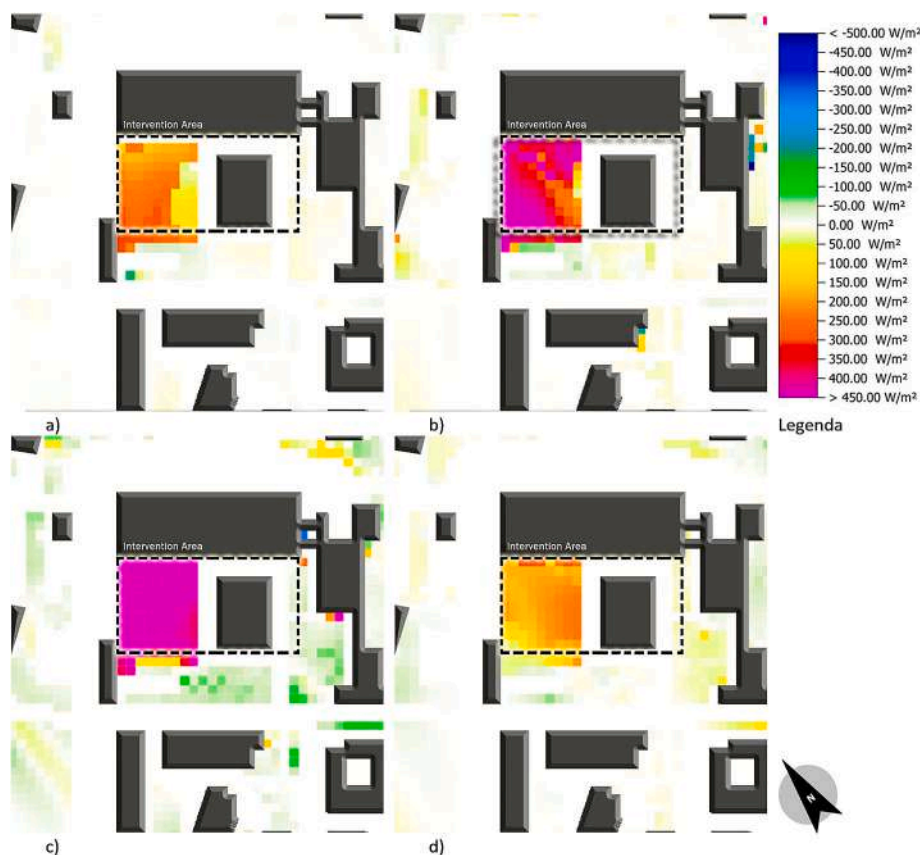


Fig. 25. Comparison of the latent heat fluxes in the parking area between the RS and AS scenarios at a) h. 9, b) h. 12, c) h. 15 and d) h. 18 of the 02/08; the frame in black dash line defines the intervention area of the parking of the University.

Fistec Laboratory station, even if the hourly values of the parameters of outdoor air temperature and solar radiation refer to different date. The simulations were performed on 2nd August, the warmest summer day, while the samples were tested during September. The comparison with the experimental data has been carried out considering the values of the 20/09 as the warmest day during monitor period of the experimental campaign. In detail, on this day in September, the maximum air temperature was 29 °C, while it was 34 °C on 2nd August. The same assessment should be done with reference to the values of solar radiation, which difference range is on the peaks almost 50 W/m² less on 20/09.

The two receptors defined in the simulation tool and used in this analysis for this comparison with the experimental results were the ones described in the previous section. The receptor #1 that is in the same position of the samples for the experimental test (the values of this receptor can be compared with the experimental data directly) and the receptor #2, placed on the center of area to provide an average indication of the behaviour of the pavement in an empty impermeable area.

As can be seen from the charts in Fig. 27, the numerical model simulation returns surface temperature values on average slightly lower than as measured in the porous block RLB of the samples, compared the trends in figure letter a) and b). The same surface peak temperature (38 °C) has been obtained in receptor #1 if compared to the experimental data.

The peak temperature of receptors #1 and #2 is recorded at respectively 36 °C and 38 °C demonstrating that the position within the simulation mesh is affected by the configuration of the environment surrounding the intervention area. A relevant difference concerns the thermal lag of the maximum temperature is released in the charts. In the sample (Fig. 27 a) the lag between maximum radiation and maximum surface temperature is almost 2.40 h, this last is reached at around at h.

15, while in the simulation the two values are around at h. 12 and at h. 15 for the solar radiation and surface temperature respectively.

Even if the average value is almost equal (around 32 °C), the main aspect to point out concerns the trends. In fact, in the sample (Fig. 27 a) the surface temperature follows the trend of the air temperature, but also it is higher more than 10 °C in respect to the air temperature. Instead, the simulation (Fig. 27 b and c) seems to maintain both the trend and the value, so the response of the porous block to solar radiation is not equal as in the specimen and there is no great difference on surface. This could be dependent on the numerical algorithm of the software on elaborating the hourly meteorological data and on the response of the soil model in the conversion of energy to latent heat due to the presence of humidity in the soil.

Despite the differences found in the two investigation methods, it can be stated that the trend of the various parameters investigated through numerical modelling is sufficiently consistent with what can be observed in the case of experimentation. The numerical modelling part remains in fact the only way to identify a possible UHI mitigation action to be applied in a hypothesis of intervention on an urban scale.

4. Conclusions

The contribution of this work is part of the current debate on climate change and on the reduction of UHI phenomenon recognized as one of the problems related to global warming. The aim is to demonstrate how the application of porous construction elements as urban pavement layer can help to mitigate and to better control passively the microclimate. In the urban planning phase, a simple choice oriented in this direction can only guarantee beneficial effects on urban scale in the case of an extensive use of solutions such as the one analysed.

This research presents the study of a recycled block to be used for the

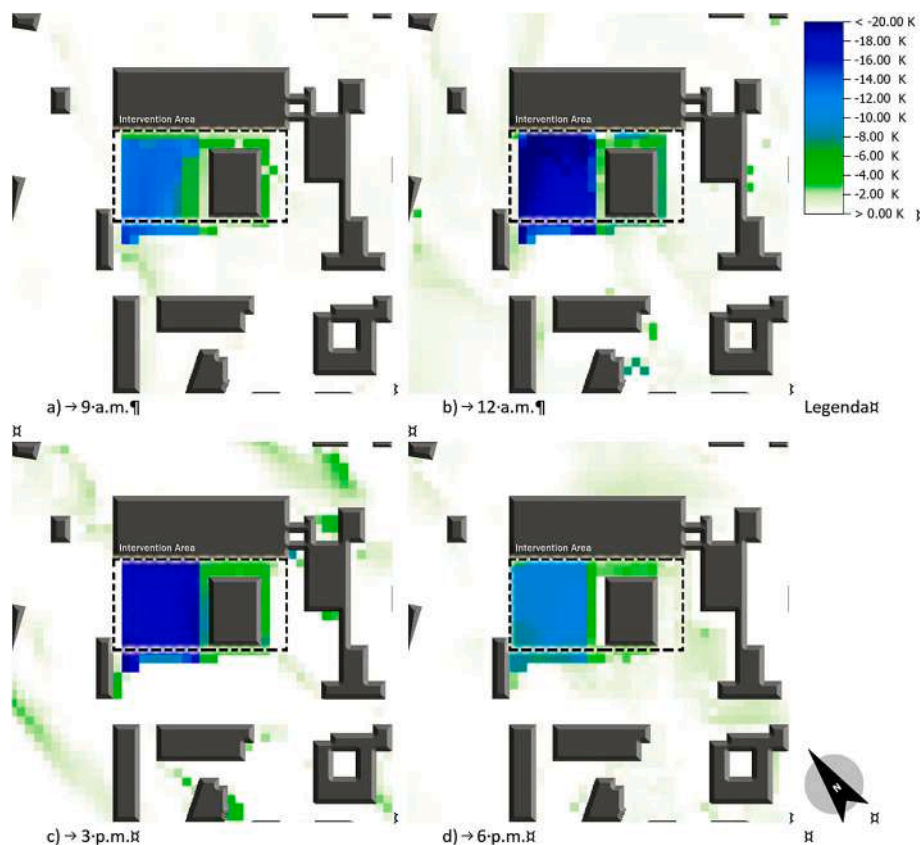


Fig. 26. Comparison of the absolute difference temperature on surface between the RS and AS scenarios at a) h. 9, b) h. 12, c) h. 15 and d) h. 18 of the 02/08; the frame in black dash line defines the intervention area of the parking of the University.

replacement of common pavement. The paper summarized the results of laboratory characterization, experimental activities on a mock-up facility and simulations, all developed in the same urban area.

As given by the experimental test, the use of these porous blocks for urban pavements underlines some remarkable notes. A porous structure is effective in the heat capacity and thermal diffusivity, 31 % lower than a standard block. Considering the average temperatures trend values on the external surfaces recorded during the monitoring period, the light colour block temperatures are always lower than the standard block or porous dark colour block, with measured peaks in the afternoon respectively 2 °C and 4 °C lower. The temperatures of a porous dark colour block are the highest during the day, precisely from late morning until evening, probably due to the different albedo and to the lower thermal conductivity if compared to the standard block. In fact, the SRI of the porous material is highly influenced by the surface colour: even if made with the same porous structure a RDB is less reflective (18 %) than TDB (32 %) and RLB (35 %). The porous block samples reveal a UHI mitigation effect showing a lower air temperature than standard pavement. In fact, a porous block (even dark coloured that leads to a higher surface temperature) heats less the air above (at 10 cm height) during the day, resulting up to 4 °C cooler from 10:00 to 17:00. The phase shift time and the thermal attenuation values given by the experimental measurements on the mock-up have been compared with the laboratory results, reporting a minimal difference with respect to the value of standard deviation. The average heat flux calculated for radiation shows higher values for RDB as the subsequent solar absorptance. In comparison to TDB, the RLB presents similar heat flux for convection and a lower heat flux for conduction from the morning to the evening, due to the higher temperature difference between the specimen's internal and external surfaces.

The simulation tests show that the presence of a significant latent heat flow causes a marked reduction in the surface temperature of the

soil and corresponds to a significant reduction in the air temperature. In fact, in comparison to a waterproof pavement in the reference case, during the day the surface temperatures of porous pavement decrease with average temperature differences ranging from −12 °C at h. 9:00 and h. 18:00, up to −20 °C at h. 12:00 and h. 15:00.

The results of the simulations are comparable to those characterized in the experimental measurement campaign, with similar daily mean (almost 32 °C) and maximum (38 °C) temperature values in the receptor at the same sample location, although the daily trend is more like that of the outdoor air. In fact, as described in the text of the paper, the pavement and its behaviour is similar to a natural permeable soil with the only difference that the surface finish influences the SRI value, making it different from those which are typical values of non-artificial pavements. Its permeability and consequently the latent heat effect.

Considering the results obtained from the experiments and the simulations, a direct comparison of the air temperature above the external surface of porous block cannot be considered reliable due to the different boundary conditions: in the specimens the temperature sensor is placed at height +0.10 m above the surface, whereas in the numerical modelling, due to the resolution of the cell grid, the temperature change is only detected above 1 m. Despite this impossibility of making a direct comparison between field experiments and numerical simulations, the latter have returned results in favour of a positive impact due to the presence of the new pavement.

However, the topic of mitigating UHI through the use of porous materials remains open to further exploration. While dark porous block contains the same porous material composition of light coloured, it is not always effective in improving the application. Therefore, a clear recommendation for practical implementation in the case of porous pavement is to consider the value of albedo, given its effect on temperatures and heat flow, as demonstrated in this research.

The research study has identified certain limitations. The evaluation

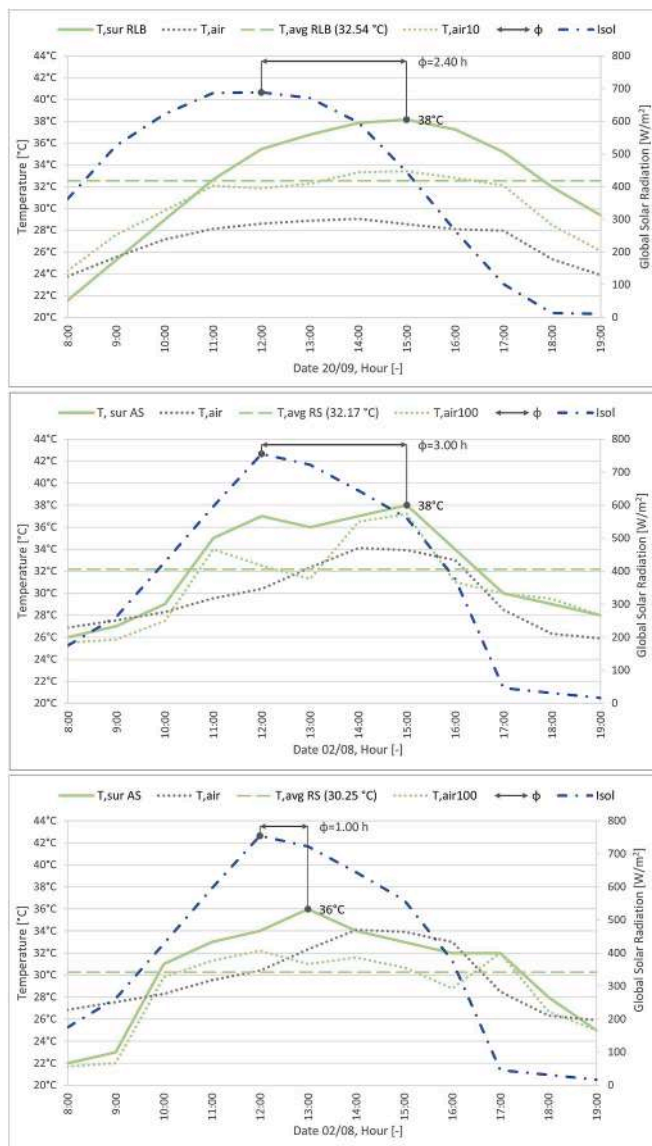


Fig. 27. Comparison between the surface temperature trend values given by a) the sample measurement and the results of receptor #1b) and #2c) by the numerical modeling with the placement of the Recycled light block in the parking area. The charts report: the thermal lag ϕ between the solar radiation peak at midday and the daily maximum temperature, the temperature of the air at surface level and + 100 cm above the surface (respectively T_{air} and T_{air100}) and the daily average temperature on sample surface (T_{avg}).

system for porous pavements encompasses a range of phenomena, including evaporation and permeability analysis, which could be incorporated into future research endeavours to facilitate more precise experimental-type evaluations of flows.

The validity of the simulation model also necessitates updating and further implementation to incorporate the modeling of evapotranspiration phenomena, calibrated with real measurements, and climate datasets collected at varying elevations near the pavement surface.

From the point of view of UHI mitigation, the porous light-coloured material RLB has proved as most effective solution, able to reduce the average external surface temperature of by 1.5–2 °C in the afternoon in respect to the standard block. Furthermore, the permeability characteristics and consequently the latent heat effect associated with evaporation are the key points of a system capable of generating beneficial

effects on temperature mitigation. At the same time, an optimal combination of these systems with adequate SRI values represents a promising solution in the control of UHI.

In the context of the use of this type of solution, it is possible to extend this application into a broader vision that encompasses other areas such as the integration of permeable paving blocks into urban design. A wide use of this solution could be constituted a comprehensive strategy with significant environmental, social, and policy-oriented implications.

Beyond mitigating the Urban Heat Island (UHI) effect through enhanced evaporative cooling and increased surface albedo, the adoption of permeable pavement contributes to broader urban sustainability goals by facilitating water infiltration and reducing surface runoff. These benefits are particularly relevant in dense metropolitan areas where impervious surfaces dominate and climatic resilience is increasingly critical.

From a planning perspective, scientific literature, urban design and policy give evidence of the implementation of permeable pavement to manage stormwater and enhance urban green spaces.

In addition, permeable paving systems can serve as a tool for public health promotion by reducing surface temperatures in pedestrian zones, thereby lowering the risk of heat-related illnesses. Their deployment in streetscapes, parks, and courtyards also offers aesthetic and functional improvements, contributing to urban livability. Given their multifunctional nature, these materials are increasingly recognized in urban policy frameworks as cost-effective and scalable interventions for enhancing climate resilience and sustainable development.

In sum, permeable paving systems represent a scalable, cost-effective intervention that intersects multiple domains of urban policy—from climate adaptation and water management to public health and spatial quality. Their growing presence in regulatory frameworks and pilot projects globally underscores their potential as a cornerstone of future-oriented urban design.

CRediT authorship contribution statement

Tiziano Dalla Mora: Writing – review & editing, Writing – original draft, Software, Resources, Methodology, Investigation, Formal analysis, Data curation, Conceptualization. **Giuseppe Emmi:** Writing – review & editing, Writing – original draft, Methodology, Investigation, Formal analysis, Conceptualization. **Paolo Ruggeri:** Resources, Investigation, Data curation. **Massimiliano De Bei:** Resources, Investigation, Data curation. **Fabio Peron:** Writing – review & editing, Visualization, Validation, Supervision, Project administration, Conceptualization.

Declaration of competing interest

The authors declare that they have no known competing financial interests or personal relationships that could have appeared to influence the work reported in this paper.

Acknowledgments

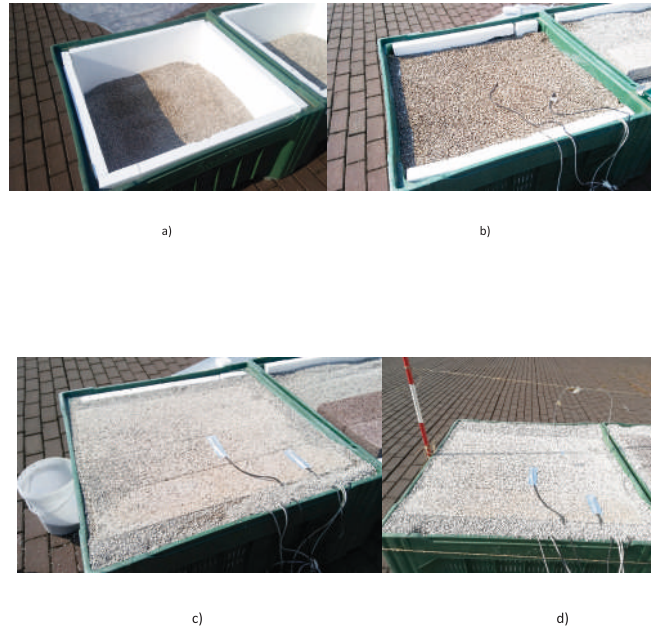
The Authors gratefully acknowledge the FAVARO1 s.r.l. company (<https://favaro1.com/it/>) for making available the Recycled blocks to develop the experimental and characterization test.

Special thanks go to Ing. Virgilio Muratore, for the numerical modelling development and analysis.

For the activities of this work the scientific equipment acquired by the IUAV University of Venice has been used; the research is developed within the activities of the BRIGAIID project, financed by the European Union's Horizon 2020 research and innovation program under grant agreement n. 700699.

Appendix

Appendix 1 – Main steps of the sample preparation: a) supply and installation of the 3 containers and arrangement of the EPS panels; b) alternating sand and sensors according to the diagram of Fig. 8 d; c) arrangement of the 3 sample types and of the external sensor #1 in the sample surface; d) placement of the external sensor #air



Appendix 2. – Specifications of the HotDisk AB 2500 TPS device.

Specifications		Values and unit
Thermal Conductivity		0.005 to 500 W/mK
Thermal Diffusivity		0.1 to 100 mm ² /s
Specific Heat Capacity		Up to 5 MJ/m ³ K
Measurement Time		1 to 1280 s
Reproducibility		Typically better than 1 %
Accuracy		Better than 5 %
Temp. Range	Standard	Ambient (Room Temp. only)
	With Furnace	Ambient to 750 °C
	With Circulator	–20 °C to 180 °C
Power Requirements		Adjusted to the line voltage in the country of use
Smallest Sample Dimensions		0.5 mm High, 2 mm Diameter (Cylindrical sample)
Sensor Types Available		- Kapton insulated with or without cable (from cryogenic temperatures up to 180 °C); - Mica insulated without cable (Room Temp. up to 750 °C).

Appendix 3. – Summary of the parameters used during the experiments with TPS device

TPS parameters	Values and unit
TCR	0.005 K ⁻¹
Temperature increase	1 – 2 K
Measurement time	80–320 s
Probing depth	17.3 – 25.3 mm
Probe radius	9.9 mm
Input power	0.14025 W
External temperature	27 °C

Appendix 4. – Technical data specifications of the pyranometer model CM 6B

Spectral range	305–2800 nm (50 % points)
Sensitivity	between 9 and 15 μV/W ^{m-2}
Impedance	70–100 Ohm
Response time	< 18 s (95 % response)

(continued on next page)

(continued)

Spectral range	305–2800 nm (50 % points)
Non-linearity	$< \pm 1.2\%$ ($< 1000 \text{ W/m}^2$)
Temperature dependence of sensitivity	$< \pm 2\%$ ($-10 \text{ }^\circ\text{C}$ to $+40 \text{ }^\circ\text{C}$)
Directional error	$< \pm 20 \text{ W/m}^2$ (beam 1000 W/m^2)
Tilt error	$< \pm 1\%$ (beam 1000 W/m^2)
Zero Offsets thermal radiation (200 Wm^{-2})	$< 15 \text{ Wm}^{-2} < 7 \text{ Wm}^{-2}$
Zero Offsets temperature change (5 K/hr)	$< \pm 4 \text{ Wm}^{-2}$

Data availability

Data will be made available on request.

References

- [1] European Climate Risk Assessment – European Environment Agency Report 01/2024. ISBN 978-92-9480-627-7 ISSN 1977-8449 doi:10.2800/204249.
- [2] IPCC, Summary for policymakers, in: Core Writing Team, H. Lee, J. Romero (Eds.), Climate Change 2023: Synthesis Report. Contribution of Working Groups I, II and III to the Sixth Assessment Report of the Intergovernmental Panel on Climate Change, IPCC, Geneva, Switzerland, 2023, pp. 1–34, doi: 10.59327/IPCC/AR6-9789291691647.001.
- [3] M.E. Gonzalez-Trevizo, K.E. Martinez-Torres, J.F. Armendariz-Lopez, M. Santamouris, G. Bojorquez-Morales, A. Luna-Leon, Research trends on environmental, energy and vulnerability impacts of Urban Heat Islands: an overview, *Energ. Buildings* 246 (2021) 111051, <https://doi.org/10.1016/j.enbuild.2021.111051>.
- [4] M. Santamouris, Recent progress on urban overheating and heat island research. Integrated assessment of the energy, environmental, vulnerability and health impact. Synergies with the global climate change, *Energ. Build.* 207 (2020), <https://doi.org/10.1016/j.enbuild.2019.109482>, 109482.
- [5] A.M. Rizwan, L.Y.C. Dennis, C. Liu, A review on the generation, determination and mitigation of Urban Heat Island, *J. Environ. Sci.* 20 (1) (2008) 120–128, [https://doi.org/10.1016/S1001-0742\(08\)60019-4](https://doi.org/10.1016/S1001-0742(08)60019-4).
- [6] M. Elena, M. Breil, S. Soriani, The heat-health nexus in the urban context: a systematic literature review exploring the socio-economic vulnerabilities and built environment characteristics, *Urban Clim.* 34 (2020) 100676, <https://doi.org/10.1016/j.uclim.2020.100676>.
- [7] N. Mueller, D. Rojas-Rueda, H. Khreis, M. Cirach, D. Andrés, J. Ballester, X. Bartoll, C. Daher, A. Deluca, C. Echave, C. Milà, S. Márquez, J. Palou, K. Pérez, C. Tonne, M. Stevenson, S. Rueda, M. Nieuwenhuijsen, Changing the urban design of cities for health: the superblock model, *Environ. Int.* 134 (2020) 105132, <https://doi.org/10.1016/j.envint.2019.105132>.
- [8] S.E. Perkins-Kirkpatrick, S.C. Lewis, Increasing trends in regional heatwaves, *Nat. Commun.* 11 (2020) 3357, <https://doi.org/10.1038/s41467-020-16970-7>.
- [9] H. Akbari, M. Pomerantz, H. Taha, Cool surfaces and shade trees to reduce energy use and improve air quality in urban areas, *Sol. Energy* 70 (3) (2001) 295–310, [https://doi.org/10.1016/S0038-092X\(00\)00089-X](https://doi.org/10.1016/S0038-092X(00)00089-X).
- [10] S. Hajat, T. Kosatky, Heat-related mortality: a review and exploration of heterogeneity, *J. Epidemiol. Commun. Health* 64 (2010) 753–760, <https://doi.org/10.1136/jech.2009.087999>.
- [11] A. Khan, S. Chatterjee, Y. Weng, Urban Heat Island Modeling for Tropical Climates, Elsevier, 2021.
- [12] B.J. He, Towards the next generation of green building for urban heat island mitigation: zero UHI impact building, *Sustain. Cities Soc.* 50 (2019), <https://doi.org/10.1016/j.scs.2019.101647>, 101647.
- [13] T.R. Oke, G.T. Johnson, D.G. Steyn, I.D. Watson, Simulation of surface urban heat islands under 'ideal' conditions at night part 2: Diagnosis of causation, *Boundary-Layer Meteorol* 56 (1991) 339–358, <https://doi.org/10.1007/BF00119211>.
- [14] F. Chen, X. Yang, W. Zhu, WRF simulations of urban heat island under hot-weather synoptic conditions: the case study of Hangzhou City, China, *Atmos. Res.* 138 (2014) 364–377, <https://doi.org/10.1016/j.atmosres.2013.12.005>.
- [15] D.N. Asimakopoulos, V.D. Assimakopoulos, N. Chrisomallidou, N. Klitsikas, D. Mangold, P. Michel, M. Santamouris, A. Tsangrassoulis, Energy and Climate in the Urban Built Environment, James and James LTD, 2001. ISBN 978-1-873936-90-0.
- [16] J. Mullaney, T. Lucke, Practical review of pervious pavement designs, *Clean (Weinh)* 42 (2014) 111–124, <https://doi.org/10.1002/clen.201300118>.
- [17] R. Ortega-Villar, L. Lizárraga-Mendiola, C. Coronel-Olivares, L.D. López-León, C. A. Bigurra-Alzati, G.A. Vázquez-Rodríguez, Effect of photocatalytic Fe2O3 nanoparticles on urban runoff pollutant removal by permeable concrete, *J. Environ. Manag.* 242 (2019) 487–495.
- [18] S. Saadeh, A. Ralla, Y. Al-Zubi, R. Wu, J. Harvey, Application of fully permeable pavements as a sustainable approach for mitigation of stormwater runoff, *Int. J. Transp. Sci. Technol.* 8 (4) (2019) 338–350, <https://doi.org/10.1016/j.ijst.2019.02.001>.
- [19] M. Kamali, M. Delkash, M. Tajrishy, Evaluation of permeable pavement responses to urban surface runoff, *J. Environ. Manag.* 187 (2017) 43–53, <https://doi.org/10.1016/j.jenvman.2016.11.027>.
- [20] F.G. Praticò, M. Giunta, C. Marino, A. Attinà, Pavement albedo and sustainability: An experimental investigation. In Proceedings of the 7th International Conference on Maintenance and Rehabilitation of Pavements and Technological Control, Auckland, New Zealand, 28–30 August 2012, 2012.
- [21] P. Starke, P. Göbel, W.G. Coldewey, Urban evaporation rates for water-permeable pavements, *Water Sci. Technol.* 62 (5) (2010) 1161–1169, <https://doi.org/10.2166/wst.2010.390>.
- [22] H. Takebayashi, M. Moriyama, Study on surface heat budget of various pavements for urban heat island mitigation, *Adv. Mater. Sci. Eng.* 2012 (2012) 523051, <https://doi.org/10.1155/2012/523051>.
- [23] P. Tataranni, C. Sangiorgi, Synthetic Aggregates for the production of innovative low impact porous layers for urban pavements, *Infrastructures* 4 (3) (2019) 48, <https://doi.org/10.3390/infrastructures4030048>.
- [24] M. Santamouris, Using cool pavements as a mitigation strategy to fight urban heat island - a review of the actual developments, *Renew. Sustain. Energy Rev.* 26 (2013) 224–240, <https://doi.org/10.1016/j.rser.2013.05.047>.
- [25] G. Battista, E.D.L. Vollarò, P. Ocioni, R.D.L. Vollarò, Effects of urban heat island mitigation strategies in an urban square: a numerical modelling and experimental investigation, *Energ. Build.* 282 (2023) 112809, <https://doi.org/10.1016/j.enbuild.2023.112809>.
- [26] T. Susca, F. Zanghirella, V. Del Fatto, Building integrated vegetation effect on micro-climate conditions for urban heat island adaptation. Lesson Learned from Turin and Rome Case Studies, *Energ. Build.* 295 (2023) 113233, <https://doi.org/10.1016/j.enbuild.2023.113233>.
- [27] M. Governatori, E.I. Cedillo-González, T. Manfredini, C. Siligardi, Solar reflective properties of porcelain tiles for UHI mitigation: effect of highly reflective frits in the engobe's formulation, *Mater. Today Sustainab.* 20 (2022) 100255, <https://doi.org/10.1016/j.mtsust.2022.100255>.
- [28] Y. Shimazaki, M. Aoki, K. Karaki, A. Yoshida, Improving outdoor human-thermal environment by optimizing the reflectance of water-retaining pavement through subjective field-based measurements, *Build. Environ.* 210 (2022) 108695, <https://doi.org/10.1016/j.buildenv.2021.108695>.
- [29] J. Chen, Z. Zhou, J. Wu, S. Hou, M. Liu, Field and laboratory measurement of albedo and heat transfer for pavement materials, *Constr. Build. Mater.* 202 (2019) 46–57, <https://doi.org/10.1016/j.conbuildmat.2019.01.028>.
- [30] A. Chiarelli, A.R. Dawson, A. García, Pavement temperature mitigation by the means of geothermally and solar heated air, *Geothermics* 68 (2017) 9–19, <https://doi.org/10.1016/j.geothermics.2017.02.002>.
- [31] N. Anting, M.F.M. Din, K. Iwao, M. Ponraj, K. Jungan, L.Y. Yong, A.J.L.M. Siang, Experimental evaluation of thermal performance of cool pavement material using waste tiles in tropical climate, *Energ. Build.* 142 (2017) 211–219, <https://doi.org/10.1016/j.enbuild.2017.03.016>.
- [32] E. Carnielo, M. Zinzi, Optical and thermal characterisation of cool asphalts to mitigate urban temperatures and building cooling demand, *Build. Environ.* 60 (2013) 56–65, <https://doi.org/10.1016/j.buildenv.2012.11.004>.
- [33] V.s. Ranieri, N. Coropulis, V. Berloco, P. Fedele, C. Intini, Laricchia, P. Colonna, The effect of different road pavement typologies on urban heat island: a case study, *Sustain. Resil. Infrastruct.* 7 (6) (2022) 803–822, <https://doi.org/10.1080/23789869.2022.2067951>.
- [34] J. Chen, R. Chu, H. Wang, L. Zhang, X. Chen, Y. Du, Alleviating urban heat island effect using high-conductivity permeable concrete pavement, *J. Clean. Prod.* 237 (2019) 117722, <https://doi.org/10.1016/j.jclepro.2019.117722>.
- [35] P. Coseola, L. Larsenb, Cooling the heat island in compact urban environments: the effectiveness of Chicago's green alley program, *Proc. Eng.* 118 (2015) 691–710, <https://doi.org/10.1016/j.proeng.2015.08.504>.
- [36] J. Stempihar, T. Pourshams-Manzouri, K.E. Kaloush, M.C. Rodezno, Porous asphalt pavement temperature effects for urban heat island analysis, *Transp. Res. Rec.* 2293 (2012) 123–130, <https://doi.org/10.3141/2293-15>.
- [37] L. Haselbach, M. Boyer, J.T. Kevern, V.R. Schaefer, Cyclic heat island impacts on traditional versus pervious concrete pavement systems, in: Transportation Research Record: Journal of the Transportation Research Board, No. 2240, Transportation Research Board of the National Academies, Washington, D.C., 2011, pp. 107–115, doi: 10.3141/2240-14.
- [38] T. Asaeda, V.T. Ca, Characteristics of permeable pavement during hot summer weather and impact on the thermal environment, *Build. Environ.* 35 (4) (2000) 363–375, [https://doi.org/10.1016/S0360-1323\(99\)00020-7](https://doi.org/10.1016/S0360-1323(99)00020-7).
- [39] H. Wu, Z. Liu, Y. Yang, S. Bai, Characterizing thermal impacts of pavement materials on urban heat island (UHI) effect, *DEStech Trans. Eng. Technol. Res.* (2017).
- [40] A. Hasheminezhad, D. King, H. Ceylan, S. Kim, Comparative life cycle assessment of natural and recycled aggregate concrete: a review, *Sci. Total Environ.* 950 (2024) 175310, <https://doi.org/10.1016/j.scitotenv.2024.175310>.

- [41] Y. Zheng, Q. Li, L. Zhou, F. Gao, Z. Deng, J. Wang, Z. Guo, H. Ding, Lifecycle assessment and lifecycle cost analysis of sustainable concrete incorporating recycled aggregates, *Sustainability* 17 (5) (2025) 1779, <https://doi.org/10.3390/su17051779>.
- [42] Y. Pu, L. Li, X. Shi, Q. Wang, A. Abomohra, A comparative life cycle assessment on recycled concrete aggregates modified by accelerated carbonation treatment and traditional methods, *Waste Manage.* (New York, N.Y.) 172 (2023) 235–244, <https://doi.org/10.1016/j.wasman.2023.10.040>.
- [43] F. Agrela, M. Rosales, M.L. Alonso, J. Ordóñez, G.M. Cuenca-Moyano, Life-cycle assessment and environmental costs of cement-based materials manufactured with mixed recycled aggregate and biomass ash, *Materials* 17 (17) (2024) 4357, <https://doi.org/10.3390/ma17174357>.
- [44] M. Santamouris, Using cool pavements as a mitigation strategy to fight urban heat island—A review of the actual developments, *Renew. Sust. Energ. Rev.* 26 (2013) 224–240, <https://doi.org/10.1016/j.rser.2013.05.047>.
- [45] E. Commission, *Evaluating the Impact of Nature-Based Solutions: A Handbook for Practitioners*, Publications Office of the European Union Luxembourg, 2021, 10.2777/244577.
- [46] European Parliament and Council of the European Union, Directive 2000/60/EC establishing a framework for Community action in the field of water policy, *Off. J. Eur. Commun. L* 327 (2000) 1–72.
- [47] European Parliament and Council of the European Union, Directive 2007/60/EC on the assessment and management of flood risks, *Off. J. Eur. Union L* 288 (2007) 27–34.
- [48] City of Copenhagen, Copenhagen Climate Adaptation Plan, 2011. https://en.klimatilpasning.dk/media/568851/copenhagen_adaption_plan.pdf (accessed 14 May 2025).
- [49] City of Portland, Environmental Services – Green Streets, 2023. <https://www.portland.gov/bes/stormwater/green-streets> (accessed 14 May 2025).
- [50] A. Mell, M. Breuste, H. Mathey, Integrating green infrastructure and ecosystem services into urban planning in Germany: the example of Berlin, *Urban For. Urban Green.* 31 (2018) 40–47, <https://doi.org/10.1016/j.ufug.2017.12.005>.
- [51] Y. Suzuki, S. Tanaka, K. Hoshino, Effects of porous pavement on stormwater runoff and urban temperature in Tokyo: a case study of Sumida City, *J. Environ. Manag.* 251 (2019) 109560, <https://doi.org/10.1016/j.jenvman.2019.109560>.
- [52] World Health Organization (WHO), Urban green spaces and health: A review of evidence, WHO Regional Office for Europe, Copenhagen, 2021. https://www.euro.who.int/_data/assets/pdf_file/0005/321971/Urban-green-spaces-and-health-review-evidence.pdf (accessed 14 May 2025).
- [53] United Nations, Sustainable Development Goal 11: Make cities inclusive, safe, resilient and sustainable, United Nations Department of Economic and Social Affairs, 2024. <https://sdgs.un.org/goals/goal11> (accessed 14 May 2025).
- [54] F. Peron, M.M. De Maria, F. Spinazzè, U. Mazzali, An analysis of the urban heat island of Venice mainland, *Sustain. Cities Soc.* 19 (2015) 300–309, <https://doi.org/10.1016/j.scs.2015.05.008>.
- [55] H.E. Beck, N.E. Zimmermann, T.R. Mcvigar, N. Vergopalan, A. Berg, E.F. Wood, Data descriptor: present and future Köppen-Geiger climate classification maps at 1-km resolution, *Sci. Data* 5 (2018), <https://doi.org/10.1038/sdata.2018.214>, 180214.
- [56] S. Esposito, R. Alilla, M.C. Beltrano, G.E. Dal Monte, L. Di Giuseppe, L. Iafrate, M. Scaglione, *Atlante italiano del clima e dei cambiamenti climatici*, Centro 29 (2014) 30.
- [57] IUAV University of Venice, Building Physics Laboratory meteorological station, Venice - Italy, <http://fistec.iuav.it/> (last access: 14 March 2025).
- [58] D. Stewart, T.R. Oke, Local climate zones for urban temperature studies, *Bull. Am. Meteorol. Soc.* (2012) 1879–1900.
- [59] Hot Disk AB, Göteborg - Sweden, <https://www.hotdiskinstruments.com/products/instruments/tps-2500-s/> (last access: 14 March 2025).
- [60] ISO 22007-2:2022 standard “Determination of thermal conductivity and thermal diffusivity - Part 2: Transient plane heat source (hot disc) method”.
- [61] ASTM, ASTM E1980-11 – Standard Practice for calculating Solar Reflectance Index of Horizontal and Low-Sloped Opaque Surfaces. Standard of the American Society for Testing and Materials, 2019.
- [62] ASTM, ASTM E1918-06 – Standard Test Method for measuring Solar Reflectance of Horizontal and Low-Sloped Surfaces in the Field. Standard of the American Society for Testing and Materials, 2015.
- [63] OTT HydroMet B.V., Kipp & Zonen instruments, Delft - The Netherlands, <https://www.kippzonen.com> (last access: 05 September 2024).
- [64] ASTM, ASTM C1371-15 – Standard Test Method for Determination of Emittance of Materials Near Room Temperature using Portable Emissometers. Standard of the American Society for Testing and Materials, 2015.
- [65] M., Bruse; (2010). ENVI-met 3.1: Updated model overview. Bochum, Germany.
- [66] S. Huttner, M. Bruse, Numerical modeling of the urban climate—a preview on ENVI-met 4.0. 7th international conference on urban climate ICUC-7, Yokohama, Japan, 2009.
- [67] S.B. Idso, J.L. Hatfield, R.J. Reginato, R.D. Jackson, Wheat yield estimation by albedo measurement, *Remote Sens. Environ.* 7 (3) (1978) 273–276.
- [68] S. Huttner, Further development and application of the 3D microclimate simulation ENVI-met, Diss. Mainz, Univ., Diss. 2012 (2012).
- [69] F. Ali-Toudert, Dependence of Outdoor Thermal Comfort on Street Design In Hot and Dry Climate, Dissertation, Albert-Ludwigs-Universität Freiburg, 2005.
- [70] L. Sthle, S. Wold, Analysis of variance (ANOVA), *Chemom. Intel. Lab. Syst.* 6 (4) (1989) 259–272, [https://doi.org/10.1016/0169-7439\(89\)80095-4](https://doi.org/10.1016/0169-7439(89)80095-4).
- [71] P. Berdahl, R. Fromberg, The thermal radiance of clear skies, *Sol. Energy* 29 (4) (1982) 299–314, [https://doi.org/10.1016/0038-092X\(82\)90245-6](https://doi.org/10.1016/0038-092X(82)90245-6).
- [72] Y. Qin, J.E. Hiller, Understanding pavement-surface energy balance and its implications on cool pavement development, *Energy Build.* 85 (2014) 389–399, <https://doi.org/10.1016/j.enbuild.2014.09.076>.